BIOCHEMISTRY
including biophysical chemistry & molecular biology

Article

pubs.acs.org/biochemistry

Structural and Functional Consequences of the Cardiac Troponin C L48Q Ca^{2+}-Sensitizing Mutation

Dan Wang,[†] Ian M. Robertson,[‡] Monica X. Li,[‡] Michelle E. McCully,[†,§] Melissa L. Crane,[‡] Zhaoxiong Luo,[†] An-Yue Tu,[†] Valerie Daggett,[†,§] Brian D. Sykes,[‡] and Michael Regnier*[,†]

[†]Department of Bioengineering, University of Washington, Seattle, Washington 98195, United States

[‡]Department of Biochemistry, University of Alberta, Edmonton, Alberta, T6G 2H7, Canada

[§]Biomolecular Structure and Design Program, University of Washington, Seattle, Washington 98195, United States

Supporting Information

ABSTRACT: Calcium binding to the regulatory domain of cardiac troponin C (cNTnC) causes a conformational change that exposes a hydrophobic surface to which troponin I (cTnI) binds, prompting a series of protein−protein interactions that culminate in muscle contraction. A number of cTnC variants that alter the Ca^{2+} sensitivity of the thin filament have been linked to disease. Tikunova and Davis engineered a series of cNTnC mutations that altered Ca^{2+} binding properties and studied the effects on the Ca^{2+} sensitivity of the thin filament and contraction [Tikunova, S. B., and Davis, J. P. (2004) *J. Biol. Chem. 279*, 35341−35352]. One of the mutations they engineered, the L48Q variant, resulted in a pronounced increase in the cNTnC Ca^{2+} binding affinity and Ca^{2+} sensitivity of cardiac muscle force development. In this work, we sought structural and mechanistic explanations for the increased Ca^{2+} sensitivity of contraction for the L48Q cNTnC variant, using an array of biophysical techniques. We found that the L48Q mutation enhanced binding of both Ca^{2+} and cTnI to cTnC. Nuclear magnetic resonance chemical shift and relaxation data provided evidence that the cNTnC hydrophobic core is more exposed with the L48Q variant. Molecular dynamics simulations suggest that the mutation disrupts a network of crucial hydrophobic interactions so that the closed form of cNTnC is destabilized. The findings emphasize the importance of cNTnC's conformation in the regulation of contraction and suggest that mutations in cNTnC that alter myofilament Ca^{2+} sensitivity can do so by modulating Ca^{2+} and cTnI binding.

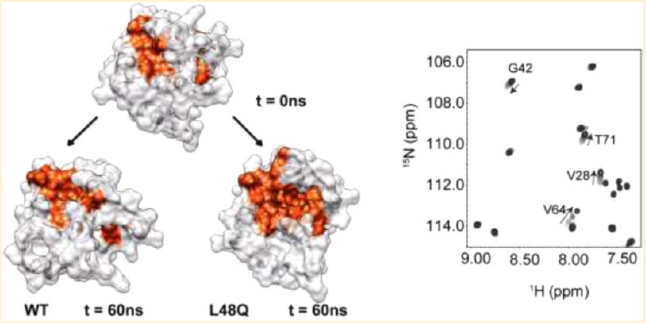

Striated muscle contraction is triggered by a transient increase in the intracellular concentration of Ca^{2+}, which binds to troponin C (TnC), the Ca^{2+}-binding subunit of the cardiac troponin (cTn) complex on thin filaments. TnC is a dumbbell-shaped protein that consists of N-terminal and C-terminal EF-hand motifs connected by a long flexible linker.[1] There are two isoforms of TnC in striated muscle: skeletal (sTnC) and cardiac (cTnC). The regulatory lobe of sTnC (sNTnC) undergoes a large structural "opening" when it binds two Ca^{2+} ions.[2] The structural change is much smaller in cNTnC upon binding Ca^{2+}, and it remains essentially "closed".[3] This difference may be the result of cNTnC having only one functional Ca^{2+} binding site (site II).[4] The C-terminus of cTnC (cCTnC) contains high-affinity Ca^{2+} binding sites, III and IV. Although these sites are thought to play primarily a structural role by anchoring the Tn complex to the thin filament, they may also be involved in the Ca^{2+} signaling pathway, because disease-related mutations in this region of cTnC affect cardiac muscle function.[5−7] cTnC interacts with the other two components of cTn: cardiac troponin I (cTnI) and cardiac troponin T (cTnT). Following the binding of Ca^{2+} to site II of cNTnC, the "switch" region of cTnI (residues 147−163, $cTnI_{147-163}$) binds to cNTnC and consequently the "inhibitory" region of cTnI (residues 112−146) dissociates from actin. The detachment of $cTnI_{112-146}$ from actin permits the increased mobility of tropomyosin over the surface of the thin filament, providing exposure of the myosin binding sites on actin and subsequently actomyosin cross-bridge formation that results in contractile force generation and cell shortening.[8,9]

A growing number of genetically identified variants (mutations) in cTn subunits associated with cardiomyopathies have been shown to alter protein−protein interactions involved in thin filament activation.[10] Thus far, at least 84 mutations in cTn proteins have been identified in patients with hypertrophic, restrictive, and dilated cardiomyopathy (HCM, RCM, and DCM, respectively).[11,12] Functional studies of HCM-associated mutations, in most cases, result in an increased Ca^{2+} sensitivity of contraction of skinned myocardium, and at least three variants are located in cTnC (A8V, C84Y, and D145E). While

Received: March 2, 2012
Revised: May 15, 2012
Published: May 16, 2012

the increase in Ca^{2+} sensitivity may not cause HCM, it is possible the augmented contractility is associated with the progression and severity of HCM over time.[13] Thus, understanding how altered Ca^{2+} binding influences cTn subunit interactions and signaling of thin filament activation could have considerable clinical relevance.

In this study, we have focused on a cTnC variant, cTnC(L48Q), which was engineered by site-directed mutagenesis to enhance the Ca^{2+} sensitivity of cTnC. This cTnC variant has not been identified in HCM patients to date; thus, it may have value in determining whether all mutations that increase the Ca^{2+} sensitivity of contraction contribute to the development of HCM. Additionally, the influence of the cTnC(L48Q) variant on the contraction and relaxation of cardiac muscle has been studied in detail. Davis and Tikunova showed that human cTnC(L48Q) increased the Ca^{2+} affinity of the Tn complex and thin filaments.[14,15] Parvatiyar et al.[16] showed it increased both the Ca^{2+} sensitivity of skinned porcine papillary contraction and the ATPase sensitivity. Recently, Kreutziger et al.[17] reported that the rat L48Q variant of cTnC had similar effects in solution and increased the Ca^{2+} sensitivity of contraction in rat trabeculae and myofibrils. It also prolonged the initial, slow phase of relaxation. Despite this wealth of functional data, the molecular mechanism for the effect of this mutation on the activation and relaxation of cardiac muscle is unknown. Additionally, little is known regarding how muations of cTnC that affect Ca^{2+} binding alter interactions with cTnI and influence thin filament activation signaling.

Leu48 makes a number of crucial hydrophobic contacts that contribute to the stabilization of a closed form of cNTnC,[1] in both the apo and Ca^{2+}-saturated states.[3] We have employed an integrative approach to understand how cTnC(L48Q) results in increased myofilament Ca^{2+} sensitivity. We used fluorescence spectroscopy, isothermal titration calorimetry (ITC), and nuclear magnetic resonance (NMR) spectroscopy to confirm that an increase in both Ca^{2+} and cTnI affinity occurs upon mutation of L48 to glutamine. The isolated cNTnC L48Q variant, cNTnC(L48Q), dimerized in a concentration-dependent manner, consistent with a more open conformation of the hydrophobic domain. The majority of cNTnC(L48Q) amide chemical shifts were located between cNTnC (predominantly closed conformation) and the cNTnC–$cTnI_{147-163}$ complex (open), suggesting that cNTnC(L48Q) is more open than cNTnC. Molecular dynamics (MD) simulations of the same partial protein constructs were employed to probe the detailed relationship among structure, dynamics, and function. In particular, multiple 70 ns simulations of cNTnC in the apo, Ca^{2+}-saturated, and $cTnI_{147-163}$-bound states were performed. The MD results suggest that the L48Q mutation increases the binding affinity of $cTnI_{147-163}$ for cNTnC by stabilizing its open conformation. Overall, the various results described here are consistent with the L48Q mutation stabilizing a more open conformation of cNTnC, which in turn enhances the binding of Ca^{2+} and cTnI to cNTnC.

METHODS

Protein Mutagenesis and Purification. Construction and expression of wild-type rat cTnC, cTnI, and cTnT in the pET24a vector have been described in a previous publication.[18] $cTnC^{C35S}$ and $cTnC(L48Q)^{C35S}$ were constructed from the rat wild-type cTnC plasmid with a primer based site-directed mutagenesis kit and confirmed by DNA sequence analysis. The plasmids for cTnC variants were then transformed into *Escherichia coli* BL21 cells, expressed, and purified. The DNA encoding cNTnC (residues 1−89) was inserted into the pET3a expression vector as previously described.[19] The L48Q mutation was engineered using a Quikchange site-directed mutagenesis kit from Stratagene (using paired 30-mer oligonucleotides, 5′-AAG GTG ATG AGA ATG CAA GGC CAG AAC CCC-3′ and 5′-GGG GTT CTG GCC TTG CAT TCT CAT CAC CTT-3′). The construct of cNTnC(L48Q) was transformed into *E. coli* BL21 cells, expressed, and purified. ^{15}N-labeled cNTnC(L48Q) protein was expressed in minimal medium enriched with $(^{15}NH_4)_2SO_4$.[20]

Fluorescent Labeling of Protein. The labeling procedure was previously described.[21,22] The C35S mutation was introduced to allow site-specific attachment of a fluorescent probe at C84. Briefly, $cTnC^{C35S}$ and $cTnC(L48Q)^{C35S}$ were first dialyzed against 1 mM DTT in a buffer containing 6 M urea, 25 mM Tris, and 1 mM ethylenediamine-*N*,*N*,*N*^{9},*N*^{9}-tetraacetic acid (EDTA) (pH 8.0); 5 mM DTT was added, and the proteins were then dialyzed against the same buffer without DTT for at least 12 h with three buffer changes. Then 100 mM IANBD ({*N*-[2-(iodoacetoxy)ethyl]-*N*-methyl}amino-7-nitrobenz-2-oxa-1,3-diazole (M_w = 406.14)) (in dimethylformamide) was added in a 3-fold molar excess over TnC^{C35S} or $cTnC(L48Q)^{C35S}$, and the protein solutions were gently shaken in the dark for >4 h at 4 °C. The labeling reaction was terminated by addition of 10 mM DTT, and the labeled protein solution was dialyzed against buffer containing 20 mM MOPS, 150 mM KCl, 3 mM $MgCl_2$, 2 mM EGTA, and 1 mM DTT (pH 7.0) to remove unreacted IANBD (three times for at least 12 h). Finally, $cTnC^{C35S}$ and $cTnC(L48Q)^{C35S}$ were labeled at C84 of cTnC with IANBD. We have demonstrated that the fluorescence probe at this position monitors cTnC N-terminal Ca^{2+} binding.[21] Labeling efficiency was calculated by determining the IANBD fluorophore to protein molar concentration ratio. The IANBD concentration in the labeled protein was determined by dividing the absorbance of the labeled protein at the maximal absorbance for the fuorophore by the extinction coefficient of IANBD (21000 M^{-1} cm^{-1}) at a wavelength of 481 nm. All protein concentrations were determined using the Bio-Rad protein assay. The final labeling efficiency was then determined to be 90%.

Reconstitution of Tn Complexes. Tn subunits cTnI and cTnT were first dialyzed separately against 6 M urea, 25 mM Tris, and 1 mM EDTA (pH 8). After dialysis, IANBD-$cTnC^{C35S}$, cTnI, and cTnT were mixed in a 1:1:1 molar ratio. After being incubated at room temperature for 30 min, the protein solution was dialyzed through a series of steps against (1) 2 M urea, 0.75 M KCl, 20 mM MOPS, 3 mM $MgCl_2$, and 1 mM $CaCl_2$ (pH 7.0), (2) 1 M urea, 0.75 M KCl, 20 mM MOPS, 3 mM $MgCl_2$, and 2 mM EGTA (pH 7.0), (3) 0.75 M KCl, 20 mM MOPS, 3 mM $MgCl_2$, and 2 mM EGTA (pH 7.0), (4) 0.5 M KCl, 20 mM MOPS, 3 mM $MgCl_2$, and 2 mM EGTA (pH 7.0), (5) 0.25 M KCl, 20 mM MOPS, 3 mM $MgCl_2$, and 2 mM EGTA (pH 7.0), and (6) 150 mM KCl, 20 mM MOPS, 3 mM $MgCl_2$, 2 mM EGTA, and 1 mM DTT (pH 7.0). All dialysis was done in the dark (without stirring) at 4 °C. Proteins that precipitated during the dialysis with decreasing KCl concentrations were removed by centrifugation.[23]

Steady-State Fluorescence Measurements. All steady-state fluorescence measurements were taken using a Perkin-Elmer LS50B luminescence spectrometer at 15 °C. IANBD fluorescence was excited at 490 nm and monitored at ∼530 nm (both bandwidths set at ∼8 nm). Protein buffer solutions

contained 20 mM MOPS, 150 mM KCl, 3 mM $MgCl_2$, 2 mM EGTA, and 1 mM DTT (pH 7.0). The fluorescence signal of 2 mL of IANBD-cTnC^{C35S} or IANBD-cTn^{C35S} (0.6 μM) was monitored with titration of microliter amounts of Ca^{2+} or cTnI in the presence (100 μM) or absence of Ca^{2+}. The free Ca^{2+} concentration was calculated using Maxchelator (http://maxchelator.stanford.edu).[24] The Ca^{2+} dependencies of conformational changes (pCa value at the half-maximal fluorescence signal change) were obtained by fitting the binding curve with the sigmoid Hill equation as previously described.[25] The reported values are the means of three to five successive titrations. Data are presented as means ± the standard error of the mean (SEM). Statistical significance was determined by a Student's t test using SigmaPlot (Systat Software Inc.). A p value of <0.05 was considered statistically significant.

Isothermal Titration Microcalorimetry. All experiments were performed using a Microcal, Inc., isothermal titration microcalorimeter (ITC-200) in the Analytical Biopharmacy Core at the University of Washington. Experimental conditions were as follows: 30 °C, 20 mM MOPS, pH 7.0, 150 mM KCl, 3 mM $MgCl_2$, 2 mM EGTA, and 1 mM $CaCl_2$. The sample cell was filled with 200 μL of 3 μM cTnI (with 1 mM Ca^{2+}) and titrated with 2 μL per injection of 50−70 μM cTnC (WT or L48Q, Ca^{2+}-saturated). A control titration of cTnC (WT or L48Q) to buffer was performed for each independent experiment. Binding parameters were calculated by the Origin-ITC data analysis software package using the single set of sites mode. All data are means ± SEM.

Sample Preparation and Data Analysis for NMR Spectroscopy. All NMR samples had starting volumes of 500 μL. The protein samples were dissolved in 100 mM KCl, 10 mM imidazole, and 0.2−0.25 mM 2,2-dimethyl-2-silapentane-5-sulfonate sodium salt (DSS) (Chenomx) with 0.01% NaN_3 in a 95% H_2O/5% D_2O mixture with 2−8 mM $CaCl_2$ (Fluka). Concentrations of cNTnC(L48Q) varied from 0.5 mM for assignment experiments to 0.1 mM for $cTnI_{147-163}$ titrations. The pH was kept between 6.7 and 7.0. All experiments were conducted on either a Varian Inova 500 MHz spectrometer or a Unity 600 MHz spectrometer. All data were collected at 30 °C. All NMR data were processed with NMRPipe[26] and visualized with NMRViewJ.[27] ^{15}N T_1, ^{15}N T_2, and NOE values were analyzed with the Rate Analysis and HetNOE modules in NMRViewJ. The analysis of titration data and dimerization data was conducted with xcrvfit (http://www.bionmr.ualberta.ca/bds/software/xcrvfit). Model-free analysis of the data was conducted using Mathematica notebooks.[28] Models were chosen using Akaike's Information Criteria (AIC),[29] and the chosen model was subjected to Monte Carlo analysis to assess errors.[30]

NMR Titrations. The titration of Ca^{2+} and $cTnI_{147-163}$ into [^{15}N]cNTnC(L48Q) was monitored by the $^1H-^{15}N$ HSQC NMR experiment. At each titration point, spectra were recorded, and the concentration-dependent chemical shift perturbations were used to determine dissociation constants. For the Ca^{2+} titration, initially Ca^{2+}-free buffer was prepared with Chelex 100 (Bio-Rad), which was used to chelate any free metal ions. The protein was run down a desalting column in the presence of EDTA. A 50 mM $CaCl_2$ stock solution was prepared and titrated into the apo-cNTnC(L48Q) NMR sample to final concentrations of 0.10, 0.15, 0.20, 0.25, 0.30, 0.35, 0.40, 0.45, 0.50, 0.60, 0.80, 1.41, and 2.63 mM. A 3.8 mM stock of $cTnI_{147-163}$ was prepared in DMSO-d_6 (Cambridge Isotopes Inc.), and the concentration of cNTnC(L48Q) was determined to be 84 μM. $cTnI_{147-163}$ was titrated into cNTnC(L48Q) to final concentrations of 7, 14, 22, 29, 36, 43, 57, 71, 85, 99, 120, 140, 173, 205, and 269 μM. The pH was kept between 6.9 and 7.0 throughout the titration via addition of 1 M HCl or 1 M NaOH.

NMR Experiments for Assignment. The $^1H-^{15}N$ HSQC NMR spectra of ^{15}N-labeled cNTnC(L48Q) were assigned for all three states of L48Q: apo, Ca^{2+}-bound, and $cTnI_{147-163}$-bound. The $^1H-^{15}N$ HSQC spectra for the different states of L48Q were assigned with the aid of the three-dimensional ^{15}N NOESY HSQC and ^{15}N TOCSY HSQC NMR experiments. The TOCSY HSQC experiment correlates intraresidue backbone amides with side chain protons, and the NOESY HSQC experiment correlates backbone amide nuclei with nearby nuclei, either intraresidue or interresidue. Through the combination of these two NMR experiments, and previously published assignments for cNTnC,[3,31] we were able to completely assign the backbone amides of cNTnC(L48Q) (Figure 4).

^{15}N Backbone Relaxation Experiments. To assess the concentration-dependent aggregation of cNTnC(L48Q)·Ca^{2+}, T_2 experiments were conducted at four protein concentrations (0.15, 0.33, 0.7, and 1.2 mM). The T_1 and NOE values were recorded with a cNTnC(L48Q)·Ca^{2+} concentration of 0.33 mM on the 500 and 600 MHz spectrometers and with a concentration of 0.15 mM on the 500 MHz spectrometer. All experiments were conducted with the same experimental parameters. T_1 values were determined using relaxation delays of 10, 50, 100, 200, 300, and 400 ms; T_2 values were acquired using relaxation delays of 10, 30, 50, 70, 90, and 110 ms. Delays between transients for T_1 and T_2 experiments was set to 3 s. The $^1H-^{15}N$ NOE experiments had a delay of 3 s without the proton saturation, and when proton saturation was on, it was set to 3 s.

Molecular Dynamics Simulations. The starting structure of the N-terminus of cTnC (cNTnC, from residue 1 to 89) and $cTnI_{147-163}$ complex was taken from model 18 of the NMR structure (PDB entry 1mxl).[31] The starting structure of cNTnC in the Ca^{2+}-saturated form was from model 14 of the NMR structure (PDB entry 1ap4).[3] Model 13 of the NMR structure (PDB entry 1spy)[3] was used for the apo-state cNTnC starting structure. The L48Q mutation was created in silico using UCSF Chimera[32] in all three structures. All-atom, explicit solvent MD simulations were performed at 15 °C (to match solution measurements in this study and previous mechanical measurements in cardiac muscle and myofibrils[17]) in the microcanonical (*NVE*, constant number of particles, volume, and total energy) ensemble using *in lucem* molecular mechanics (*il*mm)[33] and the Levitt et al. force field.[34] Starting structures, minimized for 1000 steps of steepest descent minimization, were solvated in a rectangular box of flexible three-center (F3C) water[35] with walls located at least 10 Å from any protein atom. The solvent density of the box was adjusted to 0.999129 g/mL, the experimental density for the simulation temperature of 15 °C.[36] A 2 fs time step was used, and structures were saved every 1 ps for analysis. Multiple ($n \geq 3$) simulations for the structures of cNTnC·Ca^{2+}·$cTnI_{147-163}$, cNTnC·Ca^{2+}, and cNTnC (both WT and L48Q) were performed for up to 70 ns each. Analysis of MD trajectories was performed with *il*mm.[33] Contacts between residues were defined as having a distance between two carbon atoms of ≤5.4 Å or any other non-carbon atoms of ≤4.6 Å. Distances were measured between specific atom pairs or between the centers of mass

of groups of atoms (e.g., two helices). Protein images were generated using UCSF Chimera.[32] Interhelical angles were calculated using interhlx (K. Yap, University of Toronto, Toronto, ON). The solvent accessible surface area (SASA) was calculated using the algorithm of Lee and Richards.[37] For all WT and L48Q measurements, and the cNTnC·Ca^{2+}·$cTnI_{147-163}$ simulations, $cTnI_{147-163}$ was removed from the MD trajectories so that the SASA of the hydrophobic patch residues in cNTnC could be then calculated. All error bars for results from the WT and L48Q MD simulation are based on the standard deviation in the average values of the multiple runs of simulations.

RESULTS

Titrations of Ca^{2+} and cTnI into cTnC(L48Q)$^{C35S}_{IANBD}$ and cTnC$^{C35S}_{IANBD}$ Monitored by Fluorescence Spectroscopy. To assess the Ca^{2+} binding affinity of the L48Q variant, we attached the fluoroprobe IANBD at C84 of cTnC$^{C35S}_{IANBD}$. IANBD is an environment-sensitive and sulfhydryl-reactive extrinsic fluorophore that has been widely used to label biological molecules for studies of intramolecular interactions.[22,38,39] Fluorescence labeling at C84 reports on conformational changes in cNTnC caused by both Ca^{2+} and cross-bridge binding.[40] We found that Ca^{2+} caused a dose-dependent increase in fluorescence from the IANBD-labeled cTnC, suggesting Ca^{2+} promotes a conformational change in the cTnC that leads to a decrease in the polarity of the environment around IANBD-labeled cysteine.

We compared the Ca^{2+}-dependent conformational changes of cTnC(L48Q)$^{C35S}_{IANBD}$ and cTnC$^{C35S}_{IANBD}$. As shown in the inset of Figure 1, cTnC(L48Q)$^{C35S}_{IANBD}$ underwent an ~1.33-fold maximal

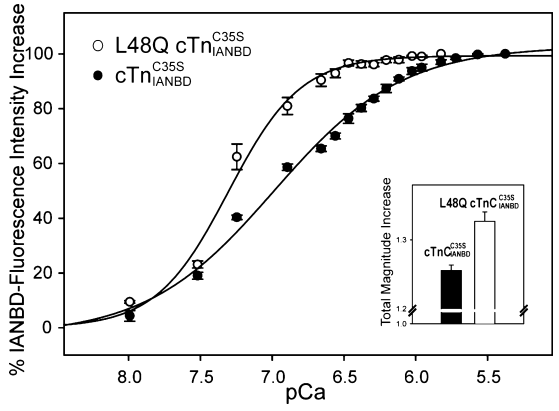

Figure 1. Effects of L48Q on the Ca^{2+}-dependent changes in the fluorescence of cTn$^{C35S}_{IANBD}$ complexes: (○) Ca^{2+} binding to L48Q cTn$^{C35S}_{IANBD}$ and (●) Ca^{2+} binding to cTn$^{C35S}_{IANBD}$. The inset shows the effects of the L48Q variant on the total magnitude of the IANBD fluorescence increase. Excitation was at 490 nm, and emission was monitored at 530 nm. The error bars represent the standard error of three to five experiments. $p < 0.05$.

increase in IANBD fluorescence when saturated with Ca^{2+} versus an ~1.25-fold increase for cTnC$^{C35S}_{IANBD}$. The enhanced magnitude of the total fluorescence change for cTnC-(L48Q)$^{C35S}_{IANBD}$ implies a larger structural change in the regulatory domain of cTnC(L48Q)$^{C35S}_{IANBD}$ upon Ca^{2+} binding. We next added cTnC(L48Q)$^{C35S}_{IANBD}$ or cTnC$^{C35S}_{IANBD}$ to wild-type cTnI and cTnT to form whole cTn complexes. Consistent with a previous report using recombinant human cTnC variants, the L48Q variant had an enhanced Ca^{2+} binding affinity.[15] The Ca^{2+} sensitivity of the fluorescence signal (reported as pCa at half-fluorescence increase) was shifted +0.32 pCa unit, from 6.99 ± 0.03 (cTn$^{C35S}_{IANBD}$) to 7.31 ± 0.03 [cTn(L48Q)$^{C35S}_{IANBD}$] (curves in Figure 1). This matches well the 0.38 pCa unit increase in Ca^{2+} sensitivity of contraction we recently reported upon exchanging cTn(L48Q)^{C35S} into skinned rat trabeculae.[17] It is also consistent with the work of Tikunova and Liu,[14] who found a 0.39 pCa unit leftward shift of pCa at half-maximal decrease in IAANS fluorescence for L48Q cTn (from pCa ~6.20 for the control protein to pCa ~6.59 for L48Q). The decreased pCa value in their results compared with ours likely results from differences in the fluoroprobe (IAANS vs IANBD), labeling strategy (at T53C of TnC C35S, T53C, C84S vs at C84 of TnC C35S), and species (human cTnC vs rat cTnC) exchanged into rat cardiac muscle.

Interactions between cTnC and cTnI play a critical role in transferring the Ca^{2+} signal to other myofilament proteins to initiate cardiac muscle contraction. Thus, in addition to examining Ca^{2+} affinity, we tested whether the L48Q variant also altered cTnI binding affinity. Binding of cTnI to cTnC was measured by titrating labeled cTnC$^{C35S}_{IANBD}$ with cTnI in the presence or absence of Ca^{2+}. Figure 2 shows the magnitude of the IANBD fluorescence change as the cTnI concentration is increased to 0.8 μM in solutions containing 0.6 μM

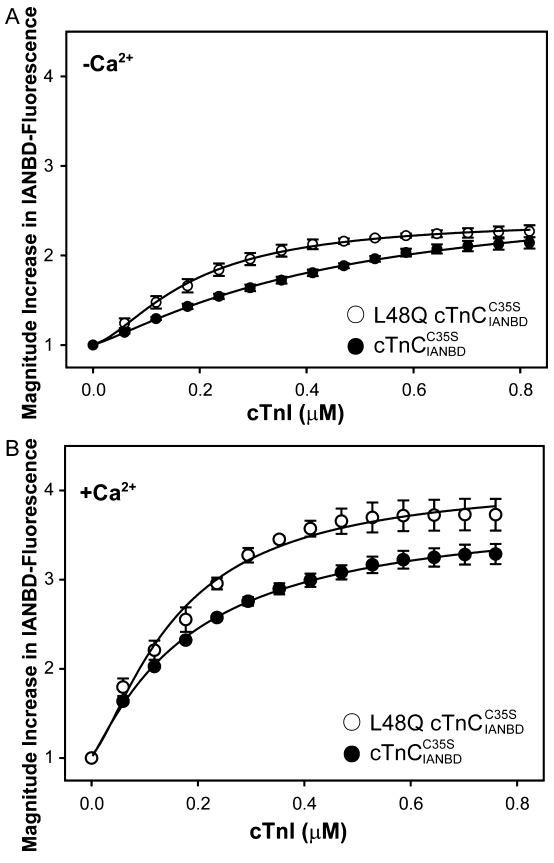

Figure 2. Effect of the L48Q variant on the binding of cTnI to cTnC$^{C35S}_{IANBD}$. The binding was assessed by measuring the changes in the IANBD fluorescence emission intensity of cTnC$^{C35S}_{IANBD}$ being titrated with cTnI (A) in the absence of Ca^{2+} ($p < 0.05$) and (B) in the presence of Ca^{2+}: (○) L48Q cTnC$^{C35S}_{IANBD}$ and (●) cTnC$^{C35S}_{IANBD}$. Excitation was at 490 nm, and emission was monitored at 530 nm. The error bars represent the standard error of three to five experiments.

dx.doi.org/10.1021/bi3003007 | Biochemistry 2012, 51, 4473−4487

cTnC(L48Q)$^{C35S}_{IANBD}$ or cTnC$^{C35S}_{IANBD}$ (control). The data demonstrate no further change in the fluorescence signal beyond 0.6 μM cTnI for either cTnC, suggesting 1:1 cTnC−cTnI binding was achieved. For both cTnC(L48Q)$^{C35S}_{IANBD}$ and the control, the magnitude of the maximal IANBD fluorescence change was greater for the Ca^{2+}-saturated states than for the apo state, indicating a larger conformational change. The amplitude of the fluorescence signal change is an indicator of the magnitude of the conformational change. This magnitude increase was compared for cTnC(L48Q)$^{C35S}_{IANBD}$ and the control in the apo and Ca^{2+}-saturated states. The maximal fluorescence increase did not differ for the apo state but was significantly increased for cTnC(L48Q)$^{C35S}_{IANBD}$ (3.73 ± 0.18-fold) compared with that of the control (3.29 ± 0.11-fold), suggesting the regulatory domain of cTnC(L48Q) is more open when bound to cTnI. cTnI appeared to bind to cTnC(L48Q)$^{C35S}_{IANBD}$·3Ca^{2+} more tightly than to cTnC$^{C35S}_{IANBD}$·3Ca^{2+}, with dissociation constants of 174 ± 8 and 198 ± 5 nM (derived from fitting the curves of normalized IANBD fluorescence change vs cTnI concentration with the sigmoid Hill equation), respectively, but these values did not differ statistically.

Binding of cTnI to cTnC Bound to Calcium by ITC. Isothermal titration calorimetry (ITC) was used to obtain a more comprehensive picture of binding of cTnI to cTnC. ITC permits monitoring of protein−protein interactions without the need for chemical modifications that may modify the interaction surface. Representative ITC data from the titration of cTnI with Ca^{2+}-saturated cTnC(L48Q) are shown in Figure 3. For each titration point, the quantity of heat released (as indicated by the negative deflection) is directly proportional to the amount of binding between the two proteins. The complete binding isotherm was obtained by plotting the integrated heat against the molar ratio of cTnC added to cTnI in the reaction cell. The stoichiometry (n), dissociation constant (K_D), and enthalpy (ΔH) of binding were obtained by fitting these data using Origin-ITC. The results from a minimum of three independent ITC binding experiments for binding of cTnC or cTnC(L48Q) to cTnI, in the presence of Ca^{2+}, suggested the binding stoichiometry was approximately 1:1 for both WT and cTnC(L48Q). Consistent with the fluorescence data, the affinity of cTnC (L48Q) for cTnI was higher than that of cTnC; K_D = 132 ± 59 nM for cTnC(L48Q), and K_D = 159 ± 91 nM for cTnC. Furthermore, the total heat released upon binding to cTnI (ΔH) for cTnC(L48Q) was −22.1 ± 1.5 kJ mol^{-1} and for cTnC −16.1 ± 3.9 kJ mol^{-1}.

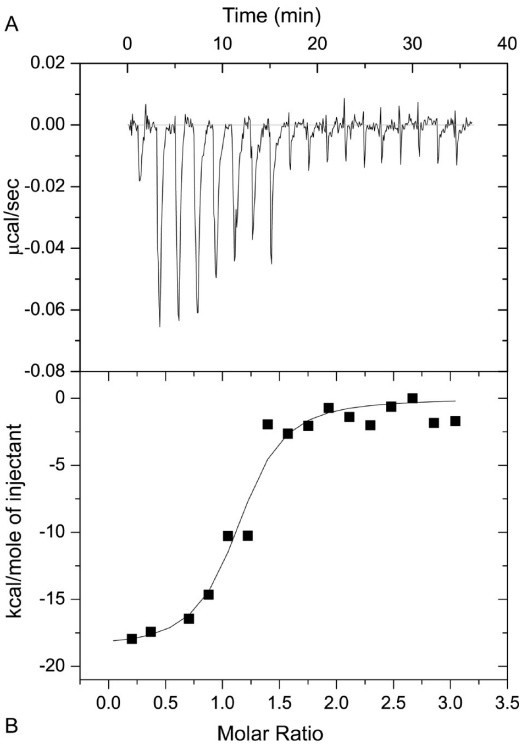

Figure 3. Microcalorimetric titration of cTnI with cTnC(L48Q) in the presence of Ca^{2+}. (A) Example trace of the titration of 3 μM cTnI with 50−70 μM cTnC(L48Q) at 30 °C. (B) Integrated heats for each injection obtained from the raw data in panel A vs the molar ratio of cTnC(L48Q) to cTnI. The data were fit to the data using a 1:1 binding model; the fit is shown with the solid line.

Titrations of Ca^{2+} and cTnI$_{147-163}$ into cNTnC(L48Q) Assessed by NMR Spectroscopy. To investigate the structural significance of L48Q on the N-lobe regulatory domain of cTnC, we used ^{15}N-labeled cNTnC(L48Q) for NMR experiments. The ^{1}H−^{15}N HSQC NMR spectrum of ^{15}N-labeled cNTnC(L48Q) was assigned for apo, Ca^{2+}-saturated, and Ca^{2+}- and cTnI$_{147-163}$-bound states using the three-dimensional ^{15}N NOESY HSQC and ^{15}N TOCSY HSQC NMR experiments (Figure 4). NMR was used to measure the affinity of cNTnC(L48Q) for Ca^{2+} and the affinity of Ca^{2+}-saturated cNTnC(L48Q) for cTnI$_{147-163}$ (Figure 5A,B). Ca^{2+} was titrated into a sample containing apo cNTnC(L48Q), and ^{1}H−^{15}N HSQC spectra were acquired at each point. The concentration-dependent chemical shift perturbations of five well-resolved resonances were used to determine the dissociation constant of Ca^{2+}, based on the global fitting method developed by Hoffman and Sykes.[41] The protocol determined a global dissociation constant that fit all the data with a minimal sum of squared error (SSE). Ca^{2+} bound to cNTnC(L48Q) with a dissociation constant of 0.6 μM (SSE = 0.055) (Figure 5C,D), ∼2-fold lower than the dissociation constant of 2.6 ± 1 μM for WT cNTnC.[42] This result is consistent with our findings for intact troponin and with those of Tikunova and Davis[15] for cTnC(L48Q), and it supports the use of the isolated domain to ascertain the effects of the L48Q mutation.

We next measured the affinity of the cTnI$_{147-163}$ switch peptide for cNTnC(L48Q)·Ca^{2+}, which is the sequence of cTnI responsible for triggering contraction through specific binding to cNTnC·Ca^{2+}.[43] The global fit yielded a cTnI$_{147-163}$ dissociation constant of 61 μM (SSE = 0.2) (Figure 5E,F), which is approximately 2 times tighter than the dissociation constant of 150 ± 10 μM measured for cNTnC by NMR.[31] The significantly weaker interaction between the fragment of cTnI (cTnI$_{147-163}$) and the isolated N-terminal domain of cTnC than what was measured by ITC and fluorescence for the full-length constructs is expected because full-length cTnI binds to both domains of cTnC with the interaction between cTnI$_{34-71}$ and cCTnC being in the nanomolar range.[44]

Comparison of Amide Chemical Shifts of cNTnC(L48Q)·Ca^{2+} with Those of Other Troponin States. The apo state of cNTnC is in a closed conformation, with its hydrophobic residues buried in the core of the protein. The NMR structure of cNTnC·Ca^{2+} indicates that a minor opening occurs when Ca^{2+} binds to site II.[3] However, cTnI$_{147-163}$ binding is required to achieve the open state of cNTnC (Figure 6). The conformation of cNTnC is described by the interhelical angles of helices A and B and helices C and D [90°

dx.doi.org/10.1021/bi3003007 | Biochemistry 2012, 51, 4473−4487

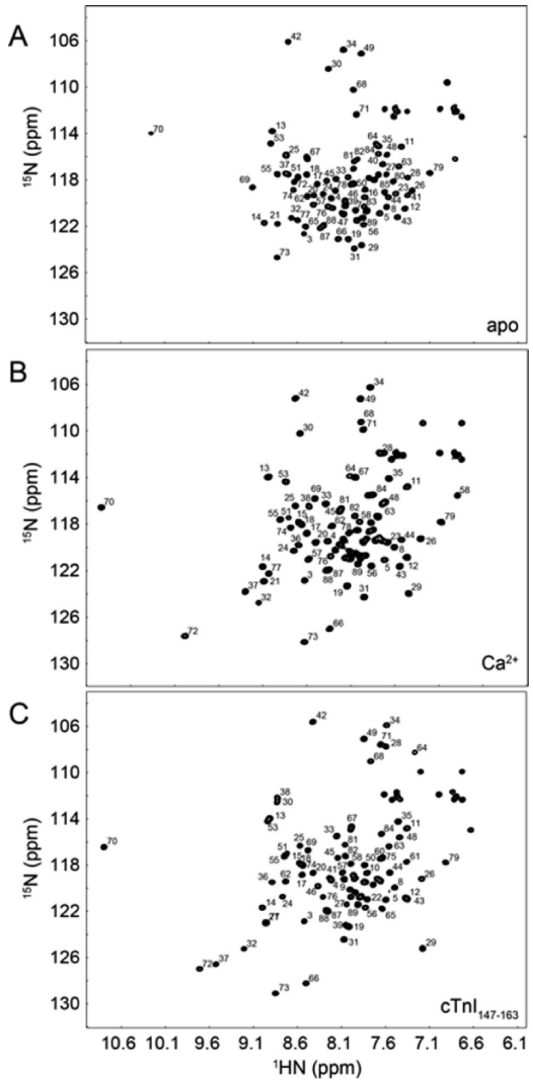

Figure 4. Assigned $^{1}H-^{15}N$ HSQC spectra of (A) apo cNTnC-(L48Q), (B) cNTnC(L48Q)·Ca^{2+}, and (C) cNTnC(L48Q)·Ca^{2+}·-$cTnI_{147-163}$. All well-resolved backbone amide peaks are labeled (side chain NH_2 groups were not assigned).

means the helices are orthogonal and thus the protein is open, and an angle near 180° indicates a more closed conformation (Figure 6)]. Although it is convenient to discuss the conformation of cNTnC in terms of angles, it must be stressed that an NMR structure is a static representation of cNTnC. cNTnC·Ca^{2+} appears to be in a dynamic equilibrium, moving between closed and open states.[45−48]

Chemical shift differences between nuclei are caused by a change in the local magnetic environment, such as by local structure or solvent exposure. Therefore, in addition to their applicability in discerning the affinity and stoichiometry of Ca^{2+} or cTnI binding, chemical shifts may be able to provide insight into the conformation of cNTnC. The Ca^{2+}-sensitizing agent, bepridil, stabilizes the open form of cNTnC in a manner similar to that of $cTnI_{147-163}$ (PDB entry 1DTL), with an interhelical angle of helices A and B of ~92°.[49] Although they are structurally distinct molecules (bepridil is a small hydrophobic molecule and $cTnI_{147-163}$ an amphipathic peptide), they induce similar amide chemical shift perturbations in the $^{1}H-^{15}N$ HSQC spectrum of cNTnC, most likely because they both stabilize the open state of cNTnC·Ca^{2+}. We overlaid the $^{1}H-^{15}N$ HSQC spectra of cNTnC·Ca^{2+}, cNTnC·Ca^{2+}·-$cTnI_{147-163}$, cNTnC·Ca^{2+}·bepridil, and cNTnC(L48Q)·Ca^{2+} to estimate the conformation of the L48Q variant (Figure 7A). The chemical shifts of cNTnC(L48Q)·Ca^{2+} were intermediate between those of cNTnC·Ca^{2+} and the complexes of bepridil or $cTnI_{147-163}$ with cNTnC·Ca^{2+}. This result suggests the L48Q mutation moves the conformational equilibrium of cNTnC·Ca^{2+} toward the open state, however, not as much as bepridil or $cTnI_{147-163}$. We recently developed a program, ORBplus, to analyze the relationship between the interhelical angles of cNTnC and amide chemical shifts.[50] ORBplus predicted that the interhelical angle of helices A and B of cNTnC(L48Q)·Ca^{2+} is approximately 10° more open (~120°) than that of cNTnC·Ca^{2+} (~130°).[50]

^{15}N T_2 and Amide Chemical Shift as a Function of Concentration. The Ca^{2+}-triggered conformational change in cNTnC is less dramatic than that in sNTnC because only one Ca^{2+} ion binds to cNTnC, whereas two Ca^{2+} ions bind to the skeletal isoform. The biological role of the exposed hydrophobic surface, in either isoform, is to promote binding of the switch region of troponin I. The exposed hydrophobic surface also serves as an interface for in vitro dimerization (in the absence of troponin I). The NMR relaxation rate R_2 ($1/T_2$) is proportional to the rotational correlation time of a protein and, hence, to its size. It has been shown that the apparent sizes of cNTnC·Ca^{2+} or sNTnC·$2Ca^{2+}$ increase as a function of concentration.[51] The dissociation constant for dimer formation (K_{dimer} = [monomer]^2/[dimer]) was previously determined to be ~7.3 mM for WT cNTnC·Ca^{2+} and ~1.3 mM for sNTnC·$2Ca^{2+}$.[51] To determine the dimerization constant of cNTnC(L48Q)·Ca^{2+}, we measured the T_2 relaxation time of L48Q at four different concentrations (1.2, 0.72, 0.33, and 0.14 mM) and plotted R_2 as a function of protein concentration[52] (Figure 7B). The dimerization constant of cNTnC-(L48Q)·Ca^{2+} was ~2 mM with an R_2 (monomer) of 6.2 s^{-1} and an R_2 (dimer) of 8.4 s^{-1} (Figure 7B). The decreased K_{dimer} of cNTnC(L48Q)·Ca^{2+} when compared to that of cNTnC·Ca^{2+} suggests that cNTnC(L48Q)·Ca^{2+} is more open than cNTnC·Ca^{2+}, but not as open as sNTnC·$2Ca^{2+}$. The concentration dependence is also shown in the amide chemical shifts at the same four concentrations (Figure 7C).

Backbone ^{15}N Relaxation Data. NMR relaxation data are a valuable source of experimental evidence of protein dynamics. The ^{15}N backbone NMR relaxation parameters T_1, T_2, and nuclear Overhauser effect (NOE) depend on the tumbling of the protein as a whole, as well as on internal motions within the protein. The measured relaxation data for cNTnC(L48Q)·Ca^{2+} at 0.33 mM are shown on a per residue basis in Figure S1 of the Supporting Information. The results indicate that cNTnC-(L48Q)·Ca^{2+} is a highly structured and rigid protein. The dramatic increase in T_1 and T_2 as well as the decrease in NOE at the C-terminus of cNTnC(L48Q)·Ca^{2+} is consistent with disorder. The average T_1^{500} (the superscript indicates the magnetic field at which the relaxation data were acquired, expressed as the frequency of ^{1}H in megahertz) for all residues was 408 ± 87 ms with an average error of 15 ms, and the average T_1^{600} was 466 ± 62 ms with an average error of 27 ms. The average T_2^{500} for all residues was 151 ± 102 ms with an average error of 8 ms, and the average T_2^{600} was 142 ± 69 ms with an average error of 7 ms. The average NOE^{500} was 0.60 ± 0.52 (average error of 0.023), and the average NOE^{600} was 0.70 ± 0.31 (average error of 0.011).

dx.doi.org/10.1021/bi3003007 | *Biochemistry* 2012, 51, 4473−4487

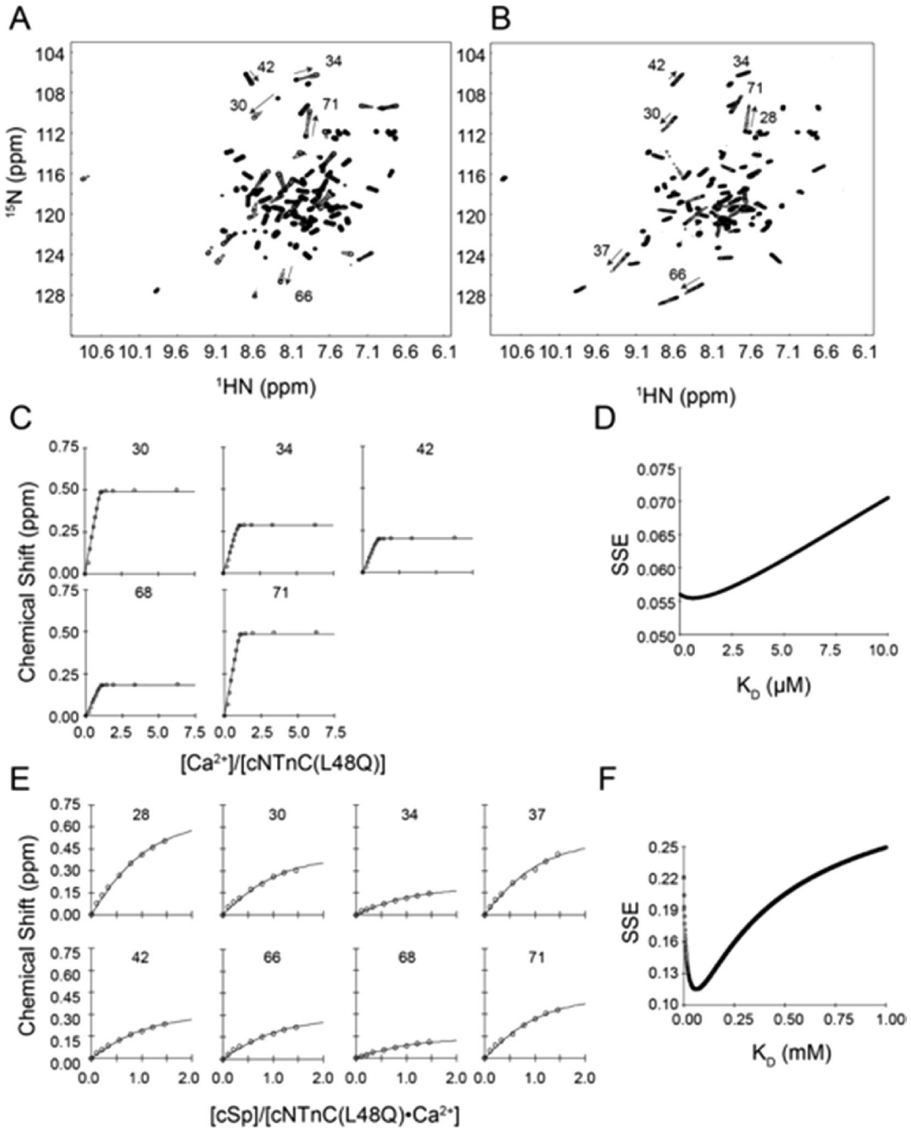

Figure 5. ^{1}H−^{15}N HSQC spectra of (A) the titration of Ca^{2+} into apo cNTnC(L48Q) and (B) the titration of $cTnI_{147-163}$ into cNTnC(L48Q)·Ca^{2+}. (C) Binding curves of the titration of Ca^{2+} into cNTnC(L48Q) that were used in the global fit to determine the dissociation constant and (D) the corresponding sum of squared error (SSE) for the global fit. (E) Representative binding curves of the titration of $cTnI_{147-163}$ into cNTnC(L48Q)·Ca^{2+} that were used in the global fit to determine the dissociation constant and (F) the corresponding SSE for the global fit.

The relaxation parameters for 0.15 mM cNTnC·Ca^{2+} have been previously published.[53] The average T_1^{500} was 440 ± 106 ms with an average error of 12 ms; the average T_2^{500} was 166 ± 82 ms with an average error of 5 ms. The average NOE^{500} was 0.57 ± 0.27 with an average error of 0.04. To directly compare cNTnC(L48Q)·Ca^{2+} with cNTnC·Ca^{2+}, we prepared a 0.15 mM sample and recorded the relaxation data at 500 MHz. The average T_1^{500} was 408 ± 97 ms with an average error of 20 ms; the average T_2^{500} was 154 ± 80 ms with an average error of 9 ms, and the average NOE was 0.70 ± 0.44 ms with an average error of 0.11 ms. We have superimposed the data from cNTnC·Ca^{2+} with those of the L48Q variant in Figure S2 of the Supporting Information.

While most of the relaxation data between cNTnC·Ca^{2+} and cNTnC(L48Q)·Ca^{2+} do not differ, inspection of residues in site I suggests that the L48Q mutation modulates the dynamics of this loop (residues 29−40). We used a suite of Mathematica notebooks to perform model-free analysis of the ^{15}N relaxation data to determine the order parameters for residues in site I.[28] Models for each residue were chosen according to Akaike's information criteria (AIC).[29] The average S^2 values obtained for loop 1 are 0.85 ± 0.11 for cNTnC(L48Q)·Ca^{2+} and 0.77 ± 0.08 for cNTnC·Ca^{2+}, implying, if anything, that the NH bond vectors in the loop are more rigid on the picosecond to nanosecond time scale in cNTnC(L48Q)·Ca^{2+}.

Effect of the L48Q Substitution on the cNTnC–$cTnI_{147-163}$ Interaction and the Position of Helix B of cNTnC. We used MD simulations to further investigate structural changes caused by the L48Q variant that may explain the experimentally observed increase in the level of binding of cTnI to cTnC. Simulations were performed for both WT cNTnC·Ca^{2+} and cNTnC(L48Q)·Ca^{2+} complexed with $cTnI_{147-163}$ (PDB entry 1MXL) at neutral pH and 15 °C and sampled over 70 ns for multiple simulations (at least five). We first investigated the residue contacts between cNTnC and $cTnI_{147-163}$. L48 is located at the end of helix B of cNTnC and makes multiple contacts with the $cTnI_{147-163}$ peptide (Figure 8A). Residues from cNTnC and $cTnI_{147-163}$ with more than

dx.doi.org/10.1021/bi3003007 | *Biochemistry* 2012, 51, 4473−4487

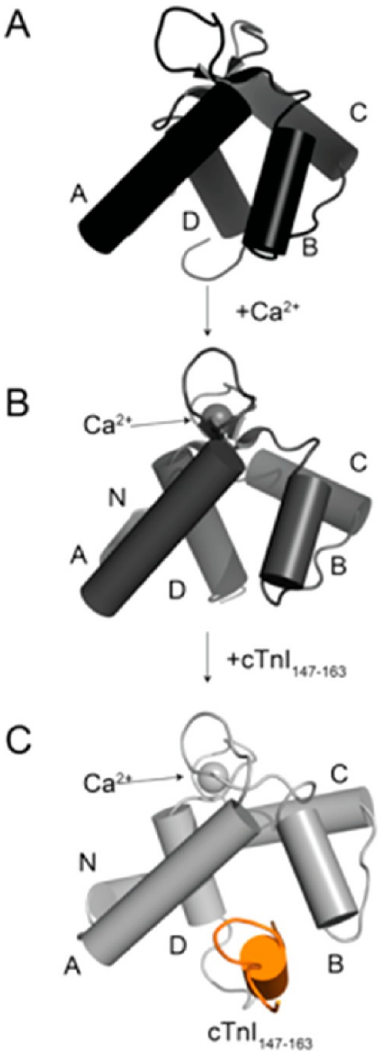

Figure 6. Conformational change of cNTnC from (A) closed in the apo state with an interhelical angle of helices A and B of ∼140° (PDB entry 1spy) through (B) slightly open in the Ca^{2+}-bound state with an interhelical angle of helices A and B of ∼130° (PDB entry 1ap4) to (C) fully open when $cTnI_{147-163}$ is bound (PDB entry 1mxl) with an interhelical angle of helices A and B of ∼102°. cNTnC is depicted in cartoon mode with the helices shown as labeled cylinders (the N helix is pointing directly into the page in panel A and is therefore not visible).

20% time in contact over entire simulations were chosen and counted as contact pairs between the two proteins. We plotted the number of contact pairs between cNTnC and $cTnI_{147-163}$ for each residue position of cNTnC to determine the overall contact map for the interaction of cNTnC with $cTnI_{147-163}$. Results are shown for WT in Figure 8B and L48Q in Figure 8C. The general pattern is similar for both cNTnC structures. The data show that residue 48 contacts the greatest number of residues in $cTnI_{147-163}$ (Figure 8B) for both proteins, suggesting this position of helix B in cNTnC is important for the interaction of cNTnC with the switch region of cTnI. However, some cNTnC residues have increased or decreased numbers of contact pairs for L48Q compared to WT, which may significantly alter the interactions between cNTnC and the cTnI switch peptide. While this merits further investigation, detailed analysis is beyond the scope of this study.

Li et al. determined that a structural deviation in WT cNTnC·Ca^{2+} associated with binding of the $cTnI_{147-163}$ peptide is the movement of helix B away from helix A.[31] The simulations of the cNTnC(L48Q)·Ca^{2+}·$cTnI_{147-163}$ complex demonstrate a significant movement of helix B for L48Q, as shown by the snapshots for simulations at 0 and 60 ns in Figure 9A (the MD movies are available as Supporting Information). This movement of helix B occurred in all of the cNTnC-(L48Q)·Ca^{2+}·$cTnI_{147-163}$ simulations, but it was not observed for any of the five WT cNTnC·Ca^{2+}·$cTnI_{147-163}$ simulations. To investigate further, we analyzed the distances and interhelical angles between helices A and B. The distances between the centers of mass of helices A and B (COMdist AB), averaged over the last 25 ns of multiple simulations, were 17.7 ± 0.7 Å for L48Q and 16.5 ± 0.7 Å for WT. The differences in COMdist AB (ΔCOMdist AB) at the end (from 45 to 70 ns) compared with the beginning of the simulations (10−25 ns) show that helices A and B moved ∼0.4 Å farther from each other for L48Q compared to WT, but the change is subtle, particularly given the dynamic nature of these helices.

To further validate the conformational change in cNTnC by the L48Q mutation, we performed MD simulations of apo and Ca^{2+}-saturated cNTnC structures (PDB entries 1SPY and 1AP4, respectively) for both WT and L48Q. In panels B and C of Figure 9, the starting structures are compared with the structures at 60 ns for cNTnC(L48Q) and cNTnC. For both apo and Ca^{2+}-saturated simulations, helix B of cNTnC(L48Q) underwent a large movement away from the core of the domain. For WT cNTnC, no significant movement of the helix was observed. Figure 9D compares helices A and B only, for all simulation structures at 60 ns versus the starting structures (90° counterclockwise rotation from the *y*-axis of the structure shown in panels A−C). From this view, it is clear that the helices A and B are generally more open for cNTnC(L48Q). This movement of the helix B was not dependent on the binding of Ca^{2+} or $cTnI_{147-163}$ in the Ca^{2+}-saturated state. Generally, cNTnC(L48Q) had greater values for the Cα rmsd of helices A and B relative to the original NMR structure from all states populated in the simulations (Figure 9E), illustrating the dynamic character and increased mobility of these helices. The difference in the motion of helix B between cNTnC-(L48Q) and cNTnC is presumably due to Gln48 at the end of helix B of the variant, which disrupts key contacts L48 makes with residues on helix A, such as F20, A23, and F27 (Figure S3 of the Supporting Information).

The interhelical angle between helices A and B (Figure 6 and Figure 9D) was used to quantify the degree of opening conformation in cNTnC. The interhelical angles of helices A and B averaged from multiple simulations were ∼87° for L48Q and ∼107° for WT, suggesting a more open conformation for L48Q cNTnC in the Ca^{2+}- and $cTnI_{147-163}$-bound state. Similar results were found for both apo and Ca^{2+}-saturated simulations; helices A and B were generally more open for L48Q than WT structures. In particular, our simulations suggest there is a decrease of ∼10° in the interhelical angle of helices A and B of L48Q compared to that of WT in the Ca^{2+}-saturated state. This magnitude of change is consistent with the prediction from ORBplus that the interhelical angle of helices A and B of cNTnC(L48Q)·Ca^{2+} is ∼10° more open than that of cNTnC·Ca^{2+}.[50]

The distance between the backbone α-carbons of M81 (on helix D) and N50 (B−C loop) was used to quantify the opening of cNTnC (Figure S4 of the Supporting Information),

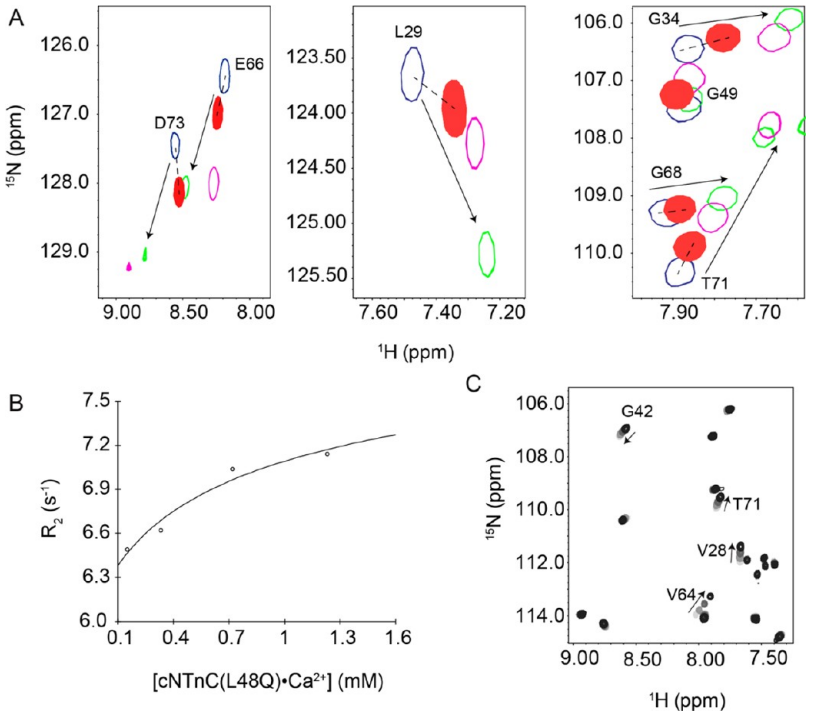

Figure 7. Characterization of the conformation of cNTnC(L48Q)·Ca^{2+} by NMR. (A) Comparison of $^{1}H-^{15}N$ HSQC spectra from cNTnC(L48Q)·Ca^{2+} (red) with cNTnC·Ca^{2+} (blue), cNTnC·Ca^{2+}·$cTnI_{147-163}$ (green), and cNTnC·Ca^{2+}·bepridil (magenta). The resonances of cNTnC(L48Q)·Ca^{2+} are shifted intermediately between those of WT cNTnC·Ca^{2+} and the $cTnI_{147-163}$- or bepridil-bound form of cNTnC. (B and C) Dependence of the average ^{15}N T_2 (B) and $^{1}H-^{15}N$ HSQC (C) as a function of cNTnC(L48Q)·Ca^{2+} concentration. In the $^{1}H-^{15}N$ HSQC spectrum, contours are colored from light gray to black as the cNTnC(L48Q)·Ca^{2+} concentration increases. Several representative residues are labeled, and arrows indicate the direction of the chemical shift as the concentration was increased.

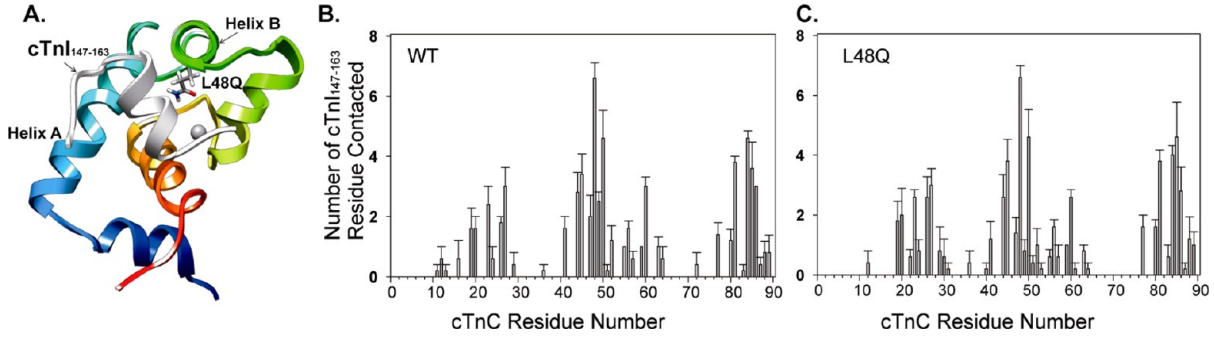

Figure 8. Interactions between cNTnC and $cTnI_{147-163}$. (A) Structure of cNTnC(L48Q)·Ca^{2+}·$cTnI_{147-163}$ (modified from PDB entry 1mxl) with residue Q48 shown as sticks, $cTnI_{147-163}$ colored white, helix A colored cyan, and helix B colored green. (B and C) Numbers of $cTnI_{147-163}$ residues that contact cNTnC (number of contact pairs) for WT and L48Q, respectively. The error bars represent the standard error from three to five simulations.

as was previously done to monitor the opening of cNTnC when $cTnI_{147-163}$ or Ca^{2+} bound to sNTnC.[31] M81−D50 distances were generally larger in the cNTnC(L48Q) mutant than in cNTnC, as calculated from all-state simulations (apo, Ca^{2+}-saturated, and $cTnI_{147-163}$-bound) (Table S1 of the Supporting Information). The increase in distance between M81 and D50 of L48Q is consistent with the interhelical angle results and the distances between helices A and B, which all indicate that the L48Q variant induced a more open state of cNTnC.

To quantify the exposure of the hydrophobic surface in cNTnC that associates with the binding with the switch region of cTnI, we selected hydrophobic residues F20, A23, F24, I26, F27, I36, L41, V44, L48, L57, M60, F77, M80, and M81 as hydrophobic patch residues. In simulations, these cNTnC residues made contacts more than 40% of time with the switch region of cTnI in cNTnC·Ca^{2+}·$cTnI_{147-163}$ (both WT and L48Q). The total SASA of the hydrophobic patch residues was greater in cNTnC·Ca^{2+}·$cTnI_{147-163}$ simulations than in cNTnC·Ca^{2+} or apo cNTnC in both WT and L48Q simulations (Table S2 of the Supporting Information), indicating the hydrophobic patch was more exposed in the presence of $cTnI_{147-163}$. This is consistent with NMR and X-ray studies showing that binding of the switch region of cTnI induces opening of cNTnC.[31,54] In addition, L48Q had a greater SASA of the hydrophobic patch area in all structures from the simulations compared to WT (Table S2 of the Supporting Information), again showing the larger hydrophobic surface area in cNTnC(L48Q). Figure 9F shows the surface rendering of structures from cNTnC·Ca^{2+} (0 and 60 ns) and

dx.doi.org/10.1021/bi3003007 | *Biochemistry* 2012, 51, 4473−4487

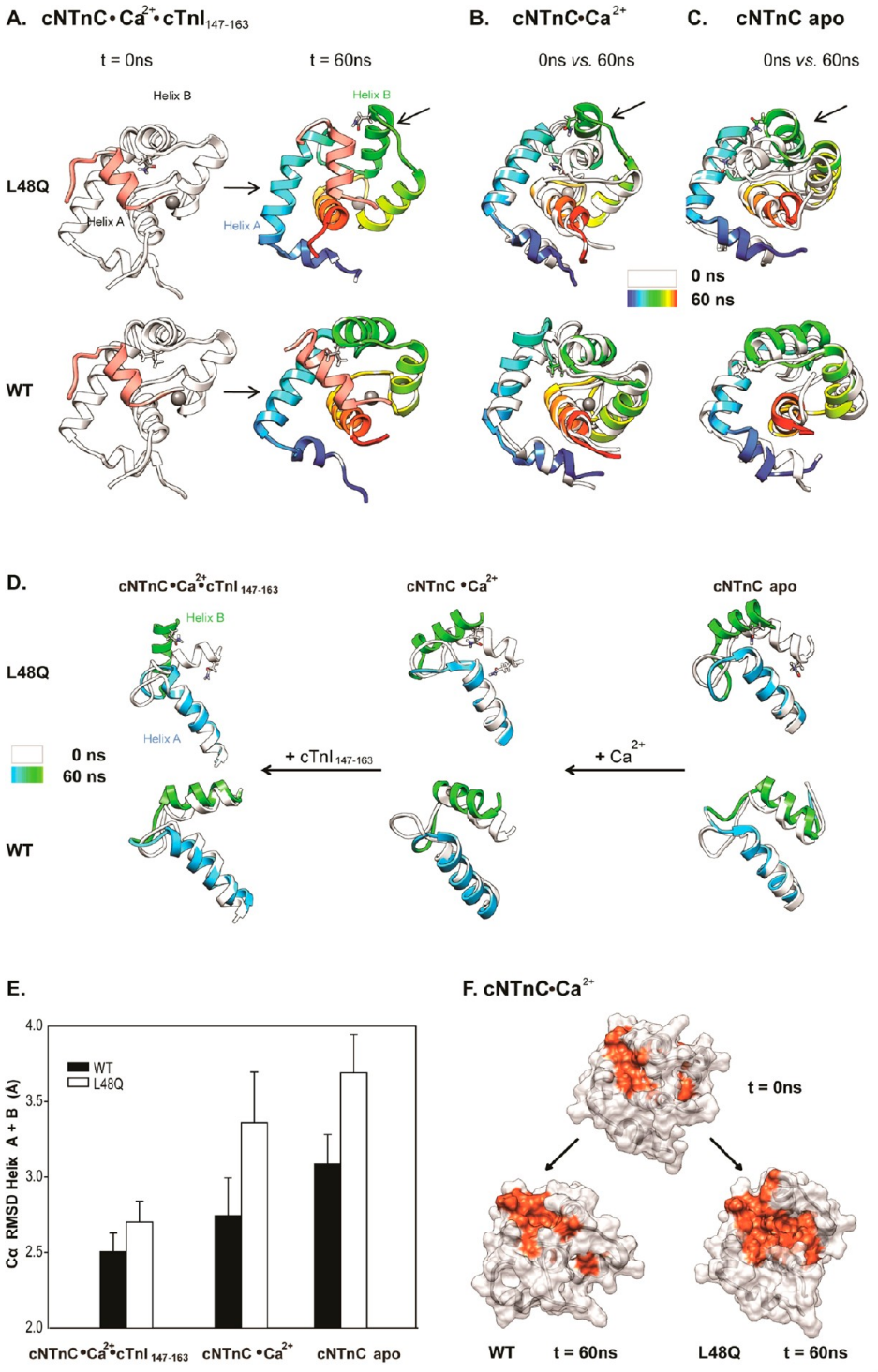

Figure 9. Effects of L48Q on the mobility of helix B in cNTnC. (A) Snapshots from cNTnC(L48Q)·Ca^{2+}·$cTnI_{147–163}$ and cNTnC·Ca^{2+}·$cTnI_{147–163}$ simulations at 0 ns (white) and 60 ns (rainbow). (B) Comparisons of 0 ns (white) vs 60 ns (rainbow) Ca^{2+}-saturated structures of cNTnC(L48Q)·Ca^{2+} (top) and cNTnC·Ca^{2+}. (C) Comparisons of 0 ns (white) vs 60 ns (rainbow) apo-state structures of cNTnC(L48Q) (top) and cNTnC. Residues L48 and Q48 are shown as sticks. (D) Helices A and B truncated from structures of L48Q and WT at 0 ns (white) and 60 ns (A helix, blue; B helix, green) of NTnC·Ca^{2+}·$cTnI_{147–163}$ (left), cNTnC·Ca^{2+} (middle), and cNTnC apo (right). The helices are shown rotated 90° to the right from the structures in panels A–C to allow a better view of the angle of helices A and B. (E) Cα rmsd for helices A and B of L48Q (white) and WT (black) averaged over all simulations of cNTnC·Ca^{2+}·$cTnI_{147–163}$, cNTnC·Ca^{2+}, and apo cNTnC. (F) Surface rendering of cNTnC·Ca^{2+} for structures from the WT (0 ns, top; 60 ns, bottom left) and L48Q (60 ns, bottom right) simulations. The hydrophobic residues (F20, A23, F24, I26, F27, I36, L41, V44, L48, L57, M60, F77, M80, and M81) are colored red, and the rest of the protein is colored white.

cNTnC(L48Q)·Ca^{2+} (60 ns) simulations. The selected hydrophobic patch residues are colored red in all structures, and the rest of the protein is colored white. Overall, the increased mobility of helix B facilitated the exposure of the hydrophobic

dx.doi.org/10.1021/bi3003007 | *Biochemistry* 2012, 51, 4473–4487

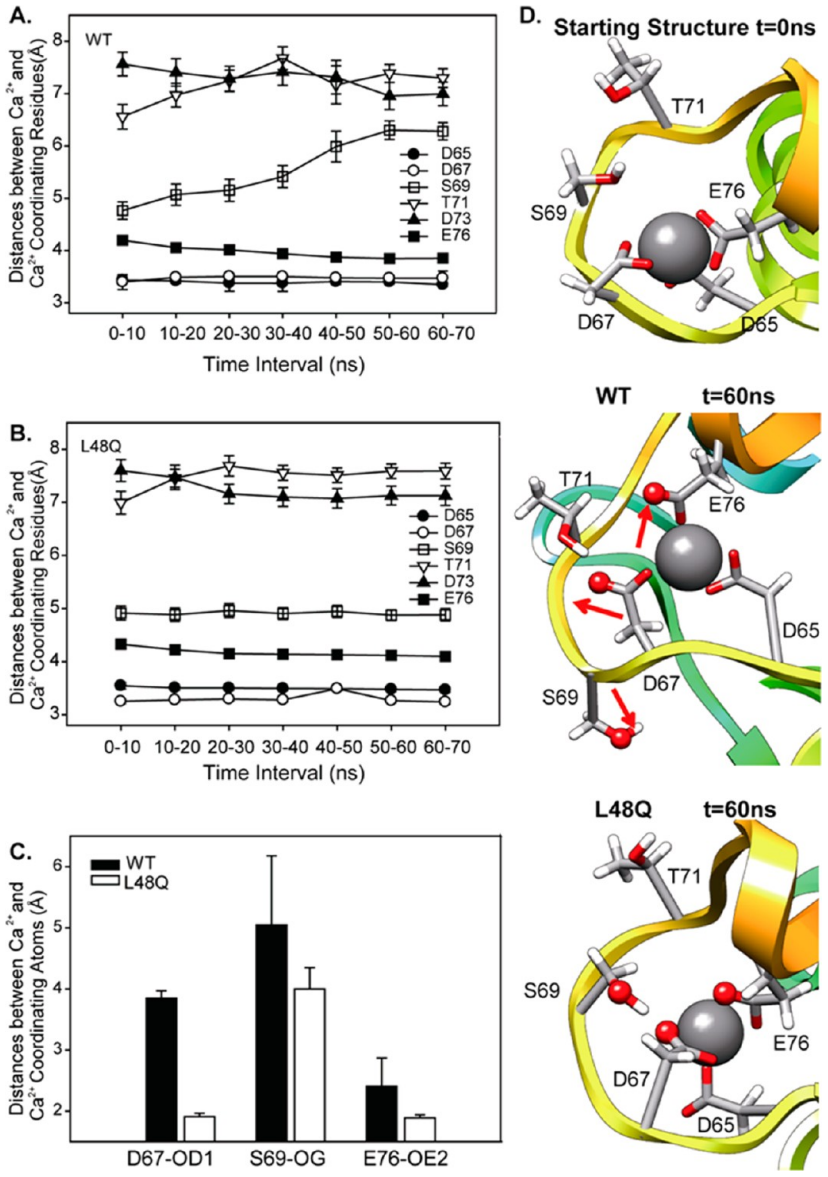

Figure 10. Ca^{2+} binding pocket at site II. (A and B) Average distances between Ca^{2+}-coordinating residues over 10 ns windows. (C) Distances between Ca^{2+} and Ca^{2+}-coordinating residues D67, S69, and E76. (D) Snapshots from L48Q and WT simulations showing the Ca^{2+} binding site compared with the starting structure (top), WT at 60 ns (middle), and L48Q at 60 ns (bottom) with Ca^{2+}-coordinating residues shown as sticks and atoms from panel C shown as spheres.

patch in cNTnC(L48Q) and disrupted the closed structure of cNTnC, which supports the idea of an increase in the binding affinity of the switch region of cTnI for cNTnC.

Effect of the L48Q Substitution on the Ca^{2+}-Coordinating Residues at Ca^{2+} Binding Site II. cTnC is one member of the EF-hand superfamily of calcium binding proteins. The EF-hand is a highly conserved (by both sequence and structure) helix−loop−helix motif with the Ca^{2+} binding loop containing 12 amino acids.[55,56] Among the 12 residues in the second Ca^{2+} binding loop (site II) of cNTnC, residues D65, D67, S69, D73, T71, and E76 at positions 1, 3, 5, 7, 9, and 12, respectively, are involved in coordination with the calcium.[57,58] Because the interactions of these residues with each other and the Ca^{2+} binding pocket itself are critical regulators of the contractile process, we also analyzed the MD simulation trajectories of cNTnC(L48Q)·Ca^{2+}·$cTnI_{147-163}$ and cNTnC·Ca^{2+}·$cTnI_{147-163}$ to examine how the L48Q substitution influences Ca^{2+} binding at cNTnC site II. The distances between the center of mass of Ca^{2+} and the Ca^{2+}-coordinating residues were calculated and averaged over time to evaluate the overall stability of the Ca^{2+} binding site (Figure 10A,B). Variability was not significant at any of the Ca^{2+}-coordinating residues, with the exception of S69, in the WT simulations. The L48Q simulations showed no significant perturbation at any residues, indicative of a very stable Ca^{2+} binding site.

Detailed coordinating information was obtained by investigating the changes in the distances between centers of mass of Ca^{2+} and individual Ca^{2+}-binding atoms, shown by examples in Figure 10C. Interestingly, in the 60 ns simulation snapshot of the WT cNTnC·Ca^{2+}·$cTnI_{147-163}$ complex, D67 OD1, E76 OE2, and S69 OG (atoms shown as red spheres in Figure 10D) pointed away from the Ca^{2+} ion. However, for the cNTnC-(L48Q)·Ca^{2+}·$cTnI_{147-163}$ complex, only D65 OD2 pointed away from the Ca^{2+} ion. Figure 10C summarizes the average distances between these atoms and Ca^{2+} throughout the simulations. When compared to the average distances between

dx.doi.org/10.1021/bi3003007 | *Biochemistry* 2012, 51, 4473−4487

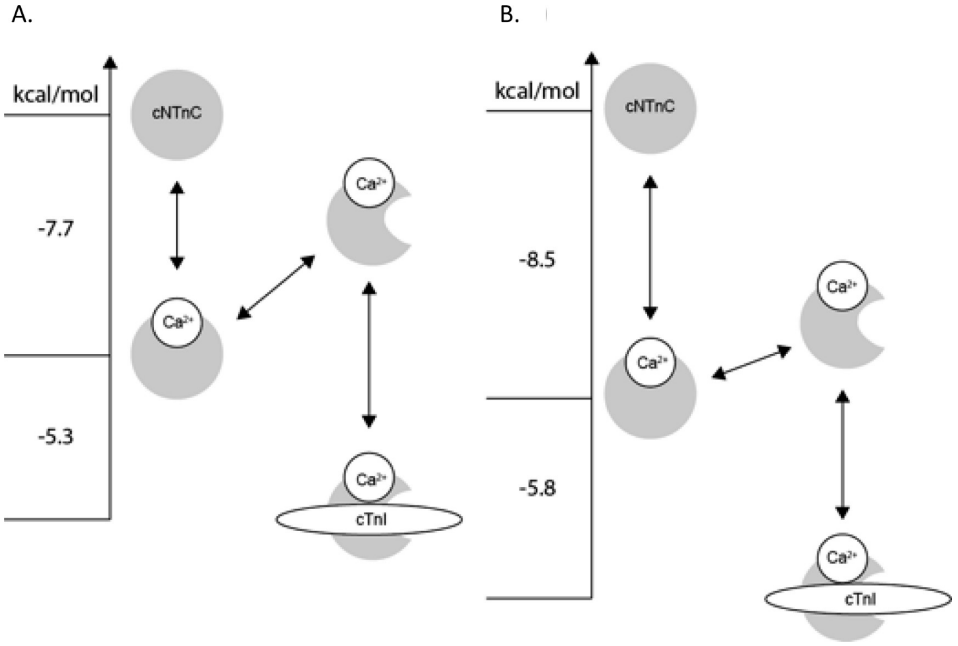

Figure 11. Energy level diagram highlighting the Ca^{2+} sensitizing mechanism of the L48Q mutation of cTnC. (A) In apo cNTnC, cNTnC is closed, once Ca^{2+} binds to cNTnC, and cNTnC oscillates between open and closed states, but the domain remains in predominantly the closed state. $cTnI_{147-163}$ binds to the open state of cNTnC to stabilize its open conformation (adapted from refs 47, 64, and 65). (B) The L48Q mutation shifts the closed-to-open equilibrium toward the open state, enhancing both the Ca^{2+} and $cTnI_{147-163}$ affinities. The free energy for panel A is from ref 47, and for panel B, the NMR data in this work are used to calculate the free energy of binding. The relationship $\Delta G^{\circ} = -RT \ln K_D$ was used to calculate the free energies.

Ca^{2+} and these atoms from the original 40 structures in the NMR ensemble of PDB entry 1MXL and those in model 18 from PDB entry 1MXL (data not shown), D67 OD1 and E76 OE2 were closer to Ca^{2+} for the L48Q variant than for WT, suggesting possible improved interactions between Ca^{2+} and these coordinating residues in the L48Q mutant. This change within the calcium binding site in the L48Q variant observed by MD simulations is consistent with our observed experimental measurements of increased Ca^{2+} binding affinity for the L48Q cTnC variant (Figure 1).

DISCUSSION

The combination of structural and functional information has been valuable for understanding the biochemical and biophysical mechanisms of proteins. Here we have used a highly integrative approach by combining fluorescence spectroscopy, microcalorimetry, NMR methodologies, and molecular dynamics simulations to determine the molecular consequences of an L48Q mutation on the conformation and dynamics of cTnC, as well as its interaction with cTnI upon Ca^{2+} binding.

It is important to elucidate the effects of cTnC modifications on its interactions with cTnI that may contribute to the change in cooperative myofilament activation. As such, knowledge of how the L48Q cTnC variant influences the cTnC−cTnI interaction will help in understanding molecular mechanisms of how altered cTn protein−protein interaction lead to changes in the Ca^{2+} sensitivity of myofilament contraction.[17] Our steady-state fluorescence spectroscopy results indicate that via interactions with cTnI, L48Q cTnC underwent greater conformational changes than the control indicated by the increased magnitude of the fluorescence signal in the presence and absence of Ca^{2+}. This increase in the extent of the L48Q cTnC−cTnI interaction suggests a strengthening of the Ca^{2+} signaling pathway between cTn subunits and tropomyosin (and actin) such that at any given subsaturating Ca^{2+} concentration, more myosin binding sites on thin filaments are available. This (for L48Q cTnC) is demonstrated in myofibrils and demembranated cardiac muscle as a faster rate of myosin binding and force development at all submaximal (but not maximal) Ca^{2+} activations.[17] A greater level of myosin binding is also demonstrated by a prolonged slow phase of relaxation in cardiac myofibrils,[17] which is thought to reflect the rate of decay of the attached myosin population during relaxation.[59] Finally, in terms of cooperative mechanisms of contractile force production, we have demonstrated that binding of myosin to actin plays a larger role in cardiac versus skeletal muscle thin filament activation[17,60−62] and that the apparent cooperativity of activation (the slope, n_H, of the force−pCa curve) is reduced by L48Q cTnC.[17] The greater conformational change of L48Q cTnC upon binding of Ca^{2+} and cTnI might lead to the exposure of the hydrophobic patch at concentrations of Ca^{2+} lower than that seen for native cTnC. This may result in a weaker dependence on allosteric activation of thin filaments by myosin in myofilaments containing L48Q cTnC.

To gain an understanding of the local structural perturbations caused by L48Q, we focused on the N-terminal domain of cTnC (cNTnC) and its interaction with Ca^{2+} and $cTnI_{147-163}$. There were several reasons why we decided to shift to the truncated forms of cTnC and cTnI. The first is that as the size of the protein increases it is more difficult to obtaining high-quality, high-resolution NMR data. More importantly, there are no significant differences in the structure of the N-domain of cTnC in cNTnC and $cNTnC{\cdot}Ca^{2+}$ versus cTnC and $cTnC{\cdot}3Ca^{2+}$,[1,3] respectively. Furthermore, the cTnC and cTnI fragments in the NMR structure of $cNTnC{\cdot}Ca^{2+}{\cdot}cTnI_{147-163}$ adopt the same conformation as in the X-ray structure of the core troponin complex ($cTnC{\cdot}3Ca^{2+}{\cdot}cTnI_{31-210}{\cdot}$

dx.doi.org/10.1021/bi3003007 | *Biochemistry* 2012, 51, 4473−4487

$cTnT_{183-288}$).[31,54] However, we cannot rule out the possibility that in addition to its local effect on the structure of cNTnC, L48Q may also have long-range effects on the structure or function of the C-terminal domain of cTnC. To explain the enhanced affinity of $cTnI_{147-163}$ for cNTnC(L48Q) observed by NMR spectroscopy, we compared the amide chemical shifts of D73, E66, L29, G34, G68, and T71 from cNTnC-(L48Q)·Ca^{2+} with the shifts of the closed state, cNTnC·Ca^{2+}, and two open states, cNTnC·Ca^{2+}·$cTnI_{147-163}$ and cNTnC·Ca^{2+}·bepridil. The averages of the chemical shifts suggest that cNTnC(L48Q)·Ca^{2+} is in a conformation somewhere between the closed and open states, closer to the closed state. Furthermore, cNTnC(L48Q) was found to dimerize more readily than cNTnC·Ca^{2+} but less readily than sNTnC·$2Ca^{2+}$, which also supports the notion that L48Q stabilizes a slightly more open state of cNTnC. The detailed information about the interaction between the $cTnI_{147-163}$ region and cNTnC will help to unambiguously trace the overall interaction between cTnC and cTnI.

The MD simulations demonstrate how the L48Q mutation causes the opening of cNTnC, with helix B swinging away from the hydrophobic core of cNTnC and remaining in that position throughout multiple 70 ns simulations. Recently, the McCammon group published a study[48] in which molecular dynamics was performed over 100 ns to assess the stability of helices A and B, and the dynamics of wild-type cNTnC. Our work builds on this and extends it to study the dynamic behavior of cNTnC(L48Q) in apo, Ca^{2+}-saturated, and $cTnI_{147-163}$-bound states in multiple long (70 ns) MD simulations. Our MD simulations predicted a decrease of approximately 10° in the interhelical angle of helices A and B of cNTnC(L48Q)·Ca^{2+}. The magnitude of this change is consistent with a recent study that used couple of different computational methods in combination with NMR data to predict that the interhelical angle of helices A and B of cNTnC(L48Q)·Ca^{2+} would decrease from ∼130° to ∼120°.[50] This structural impact is most likely the result of changing the hydrophobic Leu to the hydrophilic Gln at position 48 at the end of helix B. L48 makes key hydrophobic contacts with the side chains of residues on helix A, such as F20, A23, and F27 (Figure S3 of the Supporting Information). Overall, the results presented here suggest the L48Q mutation modulates the Ca^{2+} sensitivity of cTnC and myofilament contraction by disrupting the structure of cNTnC, destabilizing the closed conformation of cNTnC. This lowers the energetic barrier of opening, enhancing both Ca^{2+} and cTnI binding (Figure 11).

In terms of the Ca^{2+} sensitivity of cTnC, our solution spectrofluorimetry measurements demonstrate that the Ca^{2+} binding affinity (K_a) is increased by the L48Q variant for both cTnC in isolation and the cTn complex, as previously reported.[15] This increase is due primarily to a slower rate of Ca^{2+} dissociation (k_{off}), as measured for isolated cTnC, whole cTn, and reconstituted thin filaments.[15,17] S69 was the least stable Ca^{2+}-coordinating residue in the WT cNTnC MD simulations. In contrast, D67 and E76 (in addition to S69) in site II tightly coordinated Ca^{2+} in the L48Q variant more than in WT cNTnC (Figure 10C,D). Similar results have been reported for MD simulations of other EF-hand Ca^{2+} binding proteins, parvalbumin and its variants,[63] although the simulations were too short (300 ps) to make confident conclusions. L48 is located at the end of helix B (Figure 8A) and is too distant to directly affect Ca^{2+} binding at site II. Instead, the L48Q mutation causes local changes that are propagated to the calcium site. Interestingly, the Cα rmsds of helices C and D calculated from all MD simulations are 1.59 ± 0.06 Å for L48Q (six runs) and 1.88 ± 0.07 Å for WT (five runs), showing that these helices are more stable in L48Q. The exposure of the hydrophobic surface requires helices B and C to move away from the bundle of helices N, A, and D, and L48Q catalyzes the lifting movement of helix B (Movies 1 and 2 of the Supporting Information).

Although many physiological and animal model studies have revealed the functional changes between native and disease-associated cTnC mutations that may underlie the pathogenesis of heart disease, there is little information available about the structural consequences of the change in the interaction of cTnI with cTnC caused by these substitutions. Our results provide the structural, dynamic, and functional effects of the L48Q mutation of cTnC on cTnC−cTnI interactions and emphasize the importance of the conformational change in the regulatory domain of cNTnC in cardiac muscle regulation. Future studies may build on this information to determine if there is commonality of these properties for mutations associated with HCM that enhance binding of Ca^{2+} to cTn.

■ ASSOCIATED CONTENT

Supporting Information

Movies, Figures S1−S4, and Tables S1 and S2 as described in the text. This material is available free of charge via the Internet at http://pubs.acs.org.

■ AUTHOR INFORMATION

Corresponding Author

*Phone: (206) 616-4325. Fax: (206) 685-3300. E-mail: mregnier@u.washington.edu.

Author Contributions

D.W. and I.M.R. contributed equally to the research.

Funding

This work was funded by grants from the National Institutes of Health (HL65497 to M.R. and GM50789 to V.D.), the Canadian Institutes of Health Research (B.D.S.), and the Heart and Stroke Foundation of Canada (B.D.S.). I.M.R. is the recipient of a Graduate Studentship from the Alberta Heritage Foundation for Medical Research. D.W. is the recipient of the predoctoral fellowship from the American Heart Association. M.R. is an Established Investigator of the American Heart Association. M.E.M. acknowledges support by a grant from the Department of Defense through the National Defense Science and Engineering Graduate Fellowship Program for the MD studies.

Notes

The authors declare the following competing financial interest(s): M.R. holds a provisional patent application (UW ref. 45511.01US1) on cTnC L48Q overexpression to improve cardiac contractile function.

■ ACKNOWLEDGMENTS

I.M.R. and B.D.S. acknowledge helpful discussions about NMR relaxation with Professor Leo Spyracopoulos. D.W. and M.R. acknowledge all work done on Core facility instruments in the Analytical Biopharmacy Core (University of Washington), help from Dr. John Sumida, the Center for Intracellular Delivery Biologics, and the Washington State Life Sciences Discovery Fund. Computer time through the Department of Energy Office of Biological Research was provided by the National

Energy Research Scientific Computing Center, which is supported by the Office of Science of the U.S. Department of Energy under Contract DE-AC02-05CH11231.

■ ABBREVIATIONS

cTnC, intact cardiac troponin C; cNTnC, N-domain of cTnC; cTn, cardiac whole troponin; cTnC(L48Q), intact cTnC variant with the Leu48Gln mutation; cTnI, cardiac troponin I; $cTnI_{147-163}$, cTnI peptide corresponding to residues 147–163; IANBD, {*N*-[2-(iodoacetoxy)ethyl]-*N*-methyl}amino-7-nitrobenz-2-oxa-1,3-diazole; HSQC, heteronuclear single-quantum coherence; NMR, nuclear magnetic resonance; NOE, nuclear Overhauser effect; MD, molecular dynamics; WT, wild-type; PDB, Protein Data Bank; Cα rmsd, root-mean-square deviation of Cα atom coordinates from the starting structure; COMdist, distances between the centers of mass of two objects; ATMdist, distances between the centers of mass of two atoms; SASA, solvent accessible surface area.

■ REFERENCES

(1) Sia, S. K., Li, M. X., Spyracopoulos, L., Gagne, S. M., Liu, W., Putkey, J. A., and Sykes, B. D. (1997) Structure of cardiac muscle troponin C unexpectedly reveals a closed regulatory domain. *J. Biol. Chem. 272*, 18216–18221.

(2) Gagne, S. M., Tsuda, S., Li, M. X., Smillie, L. B., and Sykes, B. D. (1995) Structures of the Troponin-C Regulatory Domains in the Apo and Calcium-Saturated States. *Nat. Struct. Biol. 2*, 784–789.

(3) Spyracopoulos, L., Li, M. X., Sia, S. K., Gagne, S. M., Chandra, M., Solaro, R. J., and Sykes, B. D. (1997) Calcium-induced structural transition in the regulatory domain of human cardiac troponin C. *Biochemistry 36*, 12138–12146.

(4) Putkey, J. A., Sweeney, H. L., and Campbell, S. T. (1989) Site-Directed Mutation of the Trigger Calcium-Binding Sites in Cardiac Troponin-C. *J. Biol. Chem. 264*, 12370–12378.

(5) Baryshnikova, O. K., Robertson, I. M., Mercier, P., and Sykes, B. D. (2008) The dilated cardiomyopathy G159D mutation in cardiac troponin C weakens the anchoring interaction with troponin I. *Biochemistry 47*, 10950–10960.

(6) Ramakrishnan, S., and Hitchcock-DeGregori, S. E. (1996) Structural and functional significance of aspartic acid 89 of the troponin C central helix in Ca^{2+} signaling. *Biochemistry 35*, 15515–15521.

(7) Biesiadecki, B. J., Kobayashi, T., Walker, J. S., John Solaro, R., and de Tombe, P. P. (2007) The troponin C G159D mutation blunts myofilament desensitization induced by troponin I Ser23/24 phosphorylation. *Circ. Res. 100*, 1486–1493.

(8) Gordon, A. M., Homsher, E., and Regnier, M. (2000) Regulation of contraction in striated muscle. *Physiol. Rev. 80*, 853–924.

(9) Rarick, H. M., Tu, X. H., Solaro, R. J., and Martin, A. F. (1997) The C terminus of cardiac troponin I is essential for full inhibitory activity and Ca^{2+} sensitivity of rat myofibrils. *J. Biol. Chem. 272*, 26887–26892.

(10) Willott, R. H., Gomes, A. V., Chang, A. N., Parvatiyar, M. S., Pinto, J. R., and Potter, J. D. (2010) Mutations in troponin that cause HCM, DCM and RCM: What can we learn about thin filament function? *J. Mol. Cell. Cardiol. 48*, 882–892.

(11) Hoffmann, B., Schmidt-Traub, H., Perrot, A., Osterziel, K. J., and Gessner, R. (2001) First mutation in cardiac troponin C, L29Q, in a patient with hypertrophic cardiomyopathy. *Hum. Mutat. 17*, 524.

(12) Tardiff, J. C. (2011) Thin filament mutations: Developing an integrative approach to a complex disorder. *Circ. Res. 108*, 765–782.

(13) Gomes, A. V., and Potter, J. D. (2004) Molecular and cellular aspects of troponin cardiomyopathies. *Ann. N.Y. Acad. Sci. 1015*, 214–224.

(14) Tikunova, S. B., Liu, B., Swindle, N., Little, S. C., Gomes, A. V., Swartz, D. R., and Davis, J. P. (2010) Effect of calcium-sensitizing mutations on calcium binding and exchange with troponin C in increasingly complex biochemical systems. *Biochemistry 49*, 1975–1984.

(15) Tikunova, S. B., and Davis, J. P. (2004) Designing calcium-sensitizing mutations in the regulatory domain of cardiac troponin C. *J. Biol. Chem. 279*, 35341–35352.

(16) Parvatiyar, M. S., Pinto, J. R., Liang, J., and Potter, J. D. (2010) Predicting cardiomyopathic phenotypes by altering Ca^{2+} affinity of cardiac troponin C. *J. Biol. Chem. 285*, 27785–27797.

(17) Kreutziger, K. L., Piroddi, N., McMichael, J. T., Tesi, C., Poggesi, C., and Regnier, M. (2011) Calcium binding kinetics of troponin C strongly modulate cooperative activation and tension kinetics in cardiac muscle. *J. Mol. Cell. Cardiol. 50*, 165–174.

(18) Dong, W. J., Rosenfeld, S. S., Wang, C. K., Gordon, A. M., and Cheung, H. C. (1996) Kinetic studies of calcium binding to the regulatory site of troponin C from cardiac muscle. *J. Biol. Chem. 271*, 688–694.

(19) Pearlstone, J. R., Chandra, M., Sorenson, M. M., and Smillie, L. B. (2000) Biological function and site II Ca^{2+}-induced opening of the regulatory domain of skeletal troponin C are impaired by invariant site I or II Glu mutations. *J. Biol. Chem. 275*, 35106–35115.

(20) Li, M. X., Corson, D. C., and Sykes, B. D. (2002) Structure determination by NMR. Isotope labeling. *Methods Mol. Biol. 173*, 255–265.

(21) Marty, D. A., Regnier, M., Xu, D., and Gordon, A. M. (2001) Ca^{2+}- and cross-bridge-dependent changes in N- and C-terminal structure of troponin C in rat cardiac muscle. *Biophys. J. 80*, 360–370.

(22) Gordon, A. M., Qian, Y., Luo, Z., Wang, C. K., Mondares, R. L., and Martyn, D. A. (1997) Characterization of troponin-C interactions in skinned barnacle muscle: Comparison with troponin-C from rabbit striated muscle. *J. Muscle Res. Cell Motil. 18*, 643–653.

(23) Dong, W. J., Robinson, J. M., Stagg, S., Xing, J., and Cheung, H. C. (2003) Ca^{2+}-induced conformational transition in the inhibitory and regulatory regions of cardiac troponin I. *J. Biol. Chem. 278*, 8686–8692.

(24) Patton, C., Thompson, S., and Epel, D. (2004) Some precautions in using chelators to buffer metals in biological solutions. *Cell Calcium 35*, 427–431.

(25) George, S. E., Su, Z., Fan, D., Wang, S., and Johnson, J. D. (1996) The Fourth EF-Hand of Calmodulin and Its Helix–Loop–Helix Components: Impact on Calcium Binding and Enzyme Activation. *Biochemistry 35*, 8307–8313.

(26) Delaglio, F., Grzesiek, S., Vuister, G. W., Zhu, G., Pfeifer, J., and Bax, A. (1995) Nmrpipe: A Multidimensional Spectral Processing System Based on Unix Pipes. *J. Biomol. NMR 6*, 277–293.

(27) Johnson, B. A., and Blevins, R. A. (1994) Nmr View: A Computer-Program for the Visualization and Analysis of NMR Data. *J. Biomol. NMR 4*, 603–614.

(28) Spyracopoulos, L. (2006) A suite of Mathematica notebooks for the analysis of protein main chain N-15 NMR relaxation data. *J. Biomol. NMR 36*, 215–224.

(29) d'Auvergne, E. J., and Gooley, P. R. (2003) The use of model selection in the model-free analysis of protein dynamics. *J. Biomol. NMR 25*, 25–39.

(30) Palmer, A. G., Rance, M., and Wright, P. E. (1991) Intramolecular Motions of a Zinc Finger DNA-Binding Domain from Xfin Characterized by Proton-Detected Natural Abundance C-12 Heteronuclear NMR-Spectroscopy. *J. Am. Chem. Soc. 113*, 4371–4380.

(31) Li, M. X., Spyracopoulos, L., and Sykes, B. D. (1999) Binding of cardiac troponin-I147–163 induces a structural opening in human cardiac tropoin-C. *Biochemistry 38*, 8289–8298.

(32) Pettersen, E. F., Goddard, T. D., Huang, C. C., Couch, G. S., Greenblatt, D. M., Meng, E. C., and Ferrin, T. E. (2004) UCSF chimera: A visualization system for exploratory research and analysis. *J. Comput. Chem. 25*, 1605–1612.

(33) Beck, D. A. C., McCully, M. E., Alonso, D. O. V., and Daggett, V. (2000–2012) *in lucem* molecular mechanics (*il*mm), University of Washington, Seattle.

(34) Levitt, M., Hirshberg, M., Sharon, R., and Daggett, V. (1995) Potential-energy function and parameters for simulations of the

molecular-dynamics of proteins and nucleic-acids in solution. *Comput. Phys. Commun. 91*, 215−231.
(35) Levitt, M., Hirshberg, M., Sharon, R., Laidig, K. E., and Daggett, V. (1997) Calibration and testing of a water model for simulation of the molecular dynamics of proteins and nucleic acids in solution. *J. Phys. Chem. B 101*, 5051−5061.
(36) Kell, G. S. (1967) Precise Representation of Volume Properties of Water at 1 atm. *J. Chem. Eng. Data 12*, 66−69.
(37) Lee, B., and Richards, F. M. (1971) The interpretation of protein structures: Estimation of static accessibility. *J. Mol. Biol. 55*, 379−400.
(38) Gether, U., Lin, S., Ghanouni, P., Ballesteros, J. A., Weinstein, H., and Kobilka, B. K. (1997) Agonists induce conformational changes in transmembrane domains III and VI of the β2 adrenoceptor. *EMBO J. 16*, 6737−6747.
(39) Gether, U., Lin, S., and Kobilka, B. K. (1995) Fluorescent labeling of purified β2 adrenergic receptor. Evidence for ligand-specific conformational changes. *J. Biol. Chem. 270*, 28268−28275.
(40) Dong, W. J., and Cheung, H. C. (1996) Calcium-induced conformational change in cardiac troponin C studied by fluorescence probes attached to Cys-84. *Biochim. Biophys. Acta 1295*, 139−146.
(41) Hoffman, R. M. B., Li, M. X., and Sykes, B. D. (2005) The bindin of W7, an inhibitor of striated muscle contraction, to cardiac troponin C. *Biochemistry 44*, 15750−15759.
(42) Li, M. X., Gagne, S. M., Spyracopoulos, L., Kloks, C. P., Audette, G., Chandra, M., Solaro, R. J., Smillie, L. B., and Sykes, B. D. (1997) NMR studies of Ca^{2+} binding to the regulatory domains of cardiac and E41A skeletal muscle troponin C reveal the importance of site I to energetics of the induced structural changes. *Biochemistry 36*, 12519−12525.
(43) Tripet, B., Van Eyk, J. E., and Hodges, R. S. (1997) Mapping of a second actin-tropomyosin and a second troponin C binding site within the C terminus of troponin I, and their importance in the Ca^{2+}-dependent regulation of muscle contraction. *J. Mol. Biol. 271*, 728−750.
(44) Li, M. X., Saude, E. J., Wang, X., Pearlstone, J. R., Smillie, L. B., and Sykes, B. D. (2002) Kinetic studies of calcium and cardiac troponin I peptide binding to human cardiac troponin C using NMR spectroscopy. *Eur. Biophys. J. 31*, 245−256.
(45) Paakkonen, K., Sorsa, T., Drakenberg, T., Pollesello, P., Tilgmann, C., Permi, P., Heikkinen, S., Kilpelainen, I., and Annila, A. (2000) Conformations of the regulatory domain of cardiac troponin C examined by residual dipolar couplings. *Eur. J. Biochem. 267*, 6665−6672.
(46) Eichmueller, C., and Skrynnikov, N. R. (2007) Observation of μs time-scale protein dynamics in the presence of Ln^{3+} ions: Application to the N-terminal domain of cardiac troponin C. *J. Biomol. NMR 37*, 79−95.
(47) McKay, R. T., Saltibus, L. F., Li, M. X., and Sykes, B. D. (2000) Energetics of the induced structural change in a Ca^{2+} regulatory protein: Ca^{2+} and troponin I peptide binding to the E41A mutant of the N-domain of skeletal troponin C. *Biochemistry 39*, 12731−12738.
(48) Lindert, S., Kekenes-Huskey, P. M., Huber, G., Pierce, L., and McCammon, J. A. (2012) Dynamics and Calcium Association to the N-Terminal Regulatory Domain of Human Cardiac Troponin C: A Multiscale Computational Study. *J. Phys. Chem. B*, DOI: 10.1021/jp212173f.
(49) Li, Y., Love, M. L., Putkey, J. A., and Cohen, C. (2000) Bepridil opens the regulatory N-terminal lobe of cardiac troponin C. *Proc. Natl. Acad. Sci. U.S.A. 97*, 5140−5145.
(50) Robertson, I. M., Boyko, R. F., and Sykes, B. D. (2011) Visualizing the principal component of ^{1}H,^{15}N-HSQC NMR spectral changes that reflect protein structural or functional properties: Application to troponin C. *J. Biomol. NMR 51*, 115−122.
(51) Spyracopoulos, L., Gagne, S. M., and Sykes, B. D. (2001) in *Proceedings of the International School of Structural Biology and Magnetic Resonance* (Jardetzky, O., and Lefevre, J. F., Eds.) pp 37−44, Plenum Press, New York.
(52) Baryshnikova, O. K., and Sykes, B. D. (2006) Backbone dynamics of SDF-1α determined by NMR: Interpretation in the presence of monomer-dimer equilibrium. *Protein Sci. 15*, 2568−2578.
(53) Spyracopoulos, L., Gagne, S. M., Li, M. X., and Sykes, B. D. (1998) Dynamics and thermodynamics of the regulatory domain of human cardiac troponin C in the apo- and calcium-saturated states. *Biochemistry 37*, 18032−18044.
(54) Takeda, S., Yamashita, A., Maeda, K., and Maeda, Y. (2003) Structure of the core domain of human cardiac troponin in the Ca^{2+}-saturated form. *Nature 424*, 35−41.
(55) Lewit-Bentley, A., and Rety, S. (2000) EF-hand calcium-binding proteins. *Curr. Opin. Struct. Biol. 10*, 637−643.
(56) Marsden, B. J., Shaw, G. S., and Sykes, B. D. (1990) Calcium binding proteins. Elucidating the contributions to calcium affinity from an analysis of species variants and peptide fragments. *Biochem. Cell Biol. 68*, 587−601.
(57) Herzberg, O., and James, M. N. (1985) Structure of the calcium regulatory muscle protein troponin-C at 2.8 Å resolution. *Nature 313*, 653−659.
(58) Wilkinson, J. M., and Grand, R. J. (1975) The amino acid sequence of troponin I from rabbit skeletal muscle. *Biochem. J. 149*, 493−496.
(59) Belus, A., Piroddi, N., and Tesi, C. (2003) Mechanism of cross-bridge detachment in isometric force relaxation of skeletal and cardiac myofibrils. *J. Muscle Res. Cell Motil. 24*, 261−267.
(60) Regnier, M., Rivera, A. J., Wang, C. K., Bates, M. A., Chase, P. B., and Gordon, A. M. (2002) Thin filament near-neighbour regulatory unit interactions affect rabbit skeletal muscle steady-state force-Ca^{2+} relations. *J. Physiol. 540*, 485−497.
(61) Gordon, A. M., Rivera, A. J., Wang, C. K., and Regnier, M. (2003) Cooperative activation of skeletal and cardiac muscle. *Adv. Exp. Med. Biol. 538*, 371−379.
(62) Gillis, T. E., Martyn, D. A., Rivera, A. J., and Regnier, M. (2007) Investigation of thin filament near-neighbour regulatory unit interactions during force development in skinned cardiac and skeletal muscle. *J. Physiol. 580*, 561−576.
(63) Elkins, K. M., Gatzeva-Topalova, P. Z., and Nelson, D. J. (2001) Molecular dynamics study of Ca^{2+} binding loop variants of parvalbumin with modifications at the "gateway" position. *Protein Eng. 14*, 115−126.
(64) Paakkonen, K., Sorsa, T., Drakenberg, T., Pollesello, P., Tilgmann, C., Permi, P., Heikkinen, S., Kilpelainen, I., and Annila, A. (2000) Conformations of the regulatory domain of cardiac troponin C examined by residual dipolar couplings. *Eur. J. Biochem. 267*, 6665−6672.
(65) Sorsa, T., Pollesello, P., and Solaro, R. J. (2004) The contractile apparatus as a target for drugs against heart failure: Interaction of levosimendan, a calcium sensitiser, with cardiac troponin c. *Mol. Cell. Biochem. 266*, 87−107.